

NLRC3 is an inhibitory sensor of PI3K–mTOR pathways in cancer

Rajendra Karki^{1*}, Si Ming Man^{1*}, R. K. Subbarao Malireddi¹, Sannula Kesavardhana¹, Qifan Zhu^{1,2}, Amanda R. Burton¹, Bhesh Raj Sharma¹, Xiaopeng Qi¹, Stephane Pelletier^{1,3}, Peter Vogel⁴, Philip Rosenstiel⁵ & Thirumala-Devi Kanneganti¹

NLRs (nucleotide-binding domain and leucine-rich repeats) belong to a large family of cytoplasmic sensors that regulate an extraordinarily diverse range of biological functions. One of these functions is to contribute to immunity against infectious diseases, but dysregulation of their functional activity leads to the development of inflammatory and autoimmune diseases¹. Cytoplasmic innate immune sensors, including NLRs, are central regulators of intestinal homeostasis^{2–9}. NLRC3 (also known as CLR16.2 or NOD3) is a poorly characterized member of the NLR family and was identified in a genomic screen for genes encoding proteins bearing leucine-rich repeats (LRRs) and nucleotide-binding domains^{10,11}. Expression of *NLRC3* is drastically reduced in the tumour tissue of patients with colorectal cancer compared to healthy tissues¹², highlighting an undefined potential function for this sensor in the development of cancer. Here we show that mice lacking NLRC3 are hyper-susceptible to colitis and colorectal tumorigenesis. The effect of NLRC3 is most dominant in enterocytes, in which it suppresses activation of the mTOR signalling pathways and inhibits cellular proliferation and stem-cell-derived organoid formation. NLRC3 associates with PI3Ks and blocks activation of the PI3K-dependent kinase AKT following binding of growth factor receptors or Toll-like receptor 4. These findings reveal a key role for NLRC3 as an inhibitor of the mTOR pathways, mediating protection against colorectal cancer.

Previous studies have shown that NLRC3 functions as a negative regulator of signalling pathways activated by Toll-like receptors (TLRs) and the DNA sensor STING in response to pathogen-associated molecular patterns or to virus infection^{13,14}. The physiological role of NLRC3 has, however, remained largely unknown. Using an established mouse model of colitis-associated colorectal tumorigenesis, we investigated the role of NLRC3 in colorectal cancer. To do this, we injected mice intraperitoneally with azoxymethane, followed by three rounds of dextran sulfate sodium (DSS) treatment (Extended Data Fig. 1a). All time points referred to hereafter indicate the number of days after injection of azoxymethane. The number of tumours was quantified at day 80. Qualitative reverse-transcriptase PCR analysis revealed a reduction in the expression of the gene encoding NLRC3 in tumour tissue compared with non-tumour-associated tissue in the colon of wild-type mice 80 days after injection of azoxymethane (day 80; Extended Data Fig. 1b).

We injected cohorts of co-housed wild-type and *Nlrc3*^{-/-} mice with azoxymethane, followed by three rounds of DSS treatment, and examined the prevalence of tumours in the colon of these mice at day 80 (Extended Data Fig. 1a, c). We found that *Nlrc3*^{-/-} mice lost more body weight after the first two rounds of DSS treatment compared to wild-type mice and developed significantly more tumours (Fig. 1a–d). Histological hallmarks associated with thickening of the colon, inflammation, ulceration, hyperplasia and the extent or severity of damage were more frequently identified in the middle and distal

colon and the rectum of *Nlrc3*^{-/-} mice compared to the corresponding regions in wild-type mice (Fig. 1e, f and Extended Data Fig. 1d).

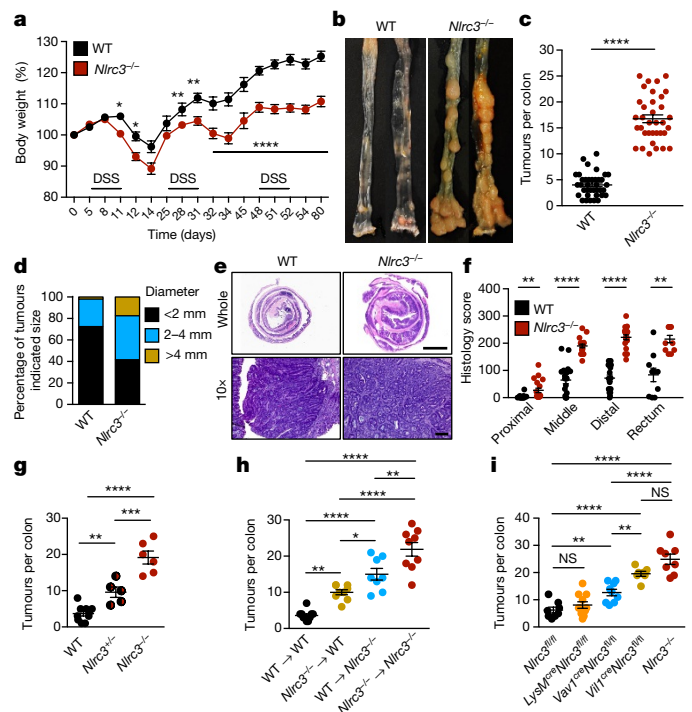


Figure 1 | NLRC3 prevents colorectal tumorigenesis. **a**, Percentage change in body weight during azoxymethane and DSS treatment; day 0 is the time of azoxymethane injection. **b**, Representative images of colon tumours in mice 80 days after injection of azoxymethane. **c**, **d**, Number (**c**) and size (**d**) of colon tumours in wild-type (WT; $n = 37$) and *Nlrc3*^{-/-} ($n = 35$) mice. **e**, **f**, Haematoxylin and eosin staining (**e**) and histological scores (**f**) of tumours in colon as shown in **b**. Scale bars, 2,500 μm (whole colon, top), 200 μm (magnified, bottom). **g**, Number of colon tumours in littermate wild-type ($n = 10$), *Nlrc3*^{+/-} ($n = 5$) and *Nlrc3*^{-/-} ($n = 6$) mice. **h**, Number of colon tumours in bone-marrow chimaera mice treated as in **b**. Wild-type mice transplanted with wild-type bone marrow ($n = 10$); *Nlrc3*^{-/-} mice transplanted with wild-type bone marrow ($n = 9$); wild-type mice transplanted with *Nlrc3*^{-/-} bone marrow ($n = 8$); and *Nlrc3*^{-/-} transplanted with *Nlrc3*^{-/-} bone marrow ($n = 9$). **i**, Number of colon tumours in littermate *Nlrc3*^{fl/fl} ($n = 8$), *LysM*^{cre}*Nlrc3*^{fl/fl} ($n = 11$), *Vav1*^{cre}*Nlrc3*^{fl/fl} ($n = 9$), *Vil1*^{cre}*Nlrc3*^{fl/fl} ($n = 7$) and *Nlrc3*^{-/-} ($n = 8$) mice treated as in **a**. Each symbol represents an individual mouse (**c**, **f**–**i**). * $P < 0.05$; ** $P < 0.01$; *** $P < 0.001$; **** $P < 0.0001$; NS, not statistically significant by one-way ANOVA (**a**, **g**–**i**) or two-tailed *t*-test (**c**, **f**). Data are from three (**a**–**f**) or two independent experiments (**g**–**i**) and are presented as mean \pm s.e.m. in **a**, **c**, **f**–**i**.

¹Department of Immunology, St. Jude Children's Research Hospital, Memphis, Tennessee 38105, USA. ²Integrated Biomedical Sciences Program, University of Tennessee Health Science Center, Memphis, Tennessee 38163, USA. ³Embryonic Stem Cell Laboratory, St. Jude Children's Research Hospital, Memphis, Tennessee 38105, USA. ⁴Animal Resources Center and the Veterinary Pathology Core, St. Jude Children's Research Hospital, Memphis, Tennessee 38105, USA. ⁵Institute of Clinical Molecular Biology, Christian-Albrechts-University Kiel, D-24105 Kiel, Germany.

*These authors contributed equally to this work.

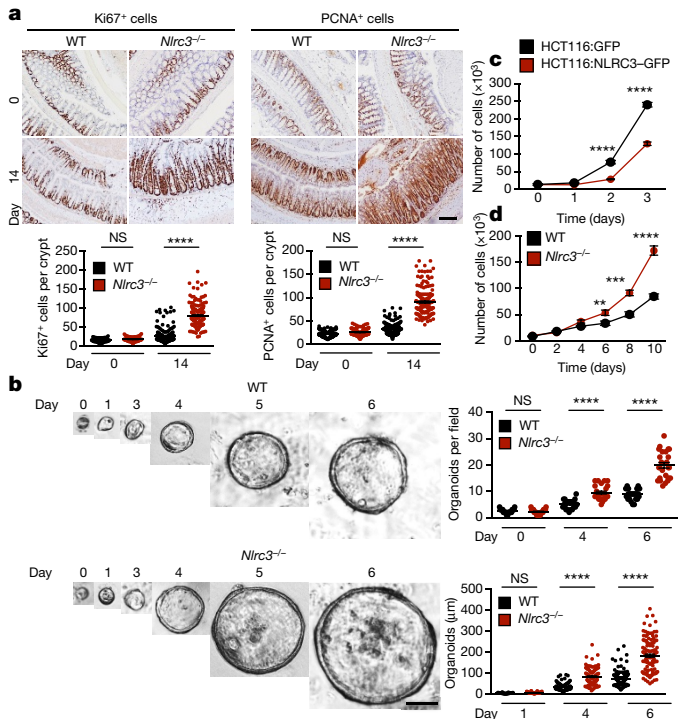


Figure 2 | NLRC3 suppresses overt proliferation. **a**, Images and quantification of the number of Ki67⁺ (left) and PCNA⁺ (right) cells in each crypt of wild-type (day 0, *n* = 5; day 14, *n* = 8) and *Nlrc3*^{-/-} (day 0, *n* = 5; day 14, *n* = 8) mice. **b**, Images (left) and quantifications (right) of the number (top) and size (bottom) of mouse intestinal organoids. **c**, Proliferation of the HCT116 cell line. **d**, Proliferation of primary mouse fibroblasts. At least 25 crypts were counted in each animal (**a**). Scale bars, 200 μm (**a**) or 50 μm (**b**). Each symbol represents one crypt (**a**) or one organoid (**b**). ***P* < 0.01; ****P* < 0.001; *****P* < 0.0001; NS, not statistically significant by two-tailed *t*-test. Data are from one experiment representative of two (**a**, **b**) or three independent experiments (**c**, **d**) and are presented as mean ± s.e.m. in **a–d**.

All *Nlrc3*^{-/-} mice suffered high-grade dysplasia, whereas wild-type mice suffered low-grade dysplasia (Extended Data Fig. 1e). We found that 63% of the *Nlrc3*^{-/-} mice were positive for adenocarcinoma in the colon, compared to 0% of the wild-type controls at day 80 (Extended Data Fig. 1f). Although NLRC3 showed a gene-dose-dependent response to azoxymethane and DSS (Fig. 1g), it does not appear to have an effect on the normal mouse intestine or colon (Extended Data Fig. 1g).

Nlrc3^{-/-} mice lost significantly more body weight and suffered more severe shortening of, and damage to, the colon after only a single round of DSS treatment compared to their wild-type counterparts (Extended Data Fig. 2a–c). Certain members of the NLR protein family can form inflammasomes, driving maturation of IL-18, a cytokine important for mediating protection against colitis-associated tumorigenesis^{2–4,15}. We did not observe differential production of IL-18 in wild-type and *Nlrc3*^{-/-} mice at day 14 or at day 80 (Extended Data Fig. 2d). Instead, production of the other inflammasome-associated cytokine IL-1β and inflammasome-independent cytokines IL-6, TNF and GCSF and the chemokines KC (also known as CXCL1), MCP-1 (also known as CCL2) and MIP-1α (also known as CCL3) was elevated in colon tissue of *Nlrc3*^{-/-} mice compared to wild-type mice at day 14 (Extended Data Fig. 2d–g). We further confirmed these results and also found increased levels of circulating IL-6, GCSF, KC and MIP-1α in the sera of *Nlrc3*^{-/-} mice compared to wild-type mice at day 14 (Extended Data Fig. 2h). The expression of IL-17 and IL-22 was also elevated in the colon tissue of *Nlrc3*^{-/-} mice compared to wild-type mice at day 14, whereas the expression of IL-23, IFNβ and IFNγ remained unchanged (Extended Data Fig. 3a). Consistent with the observation that *Nlrc3*^{-/-} mice had

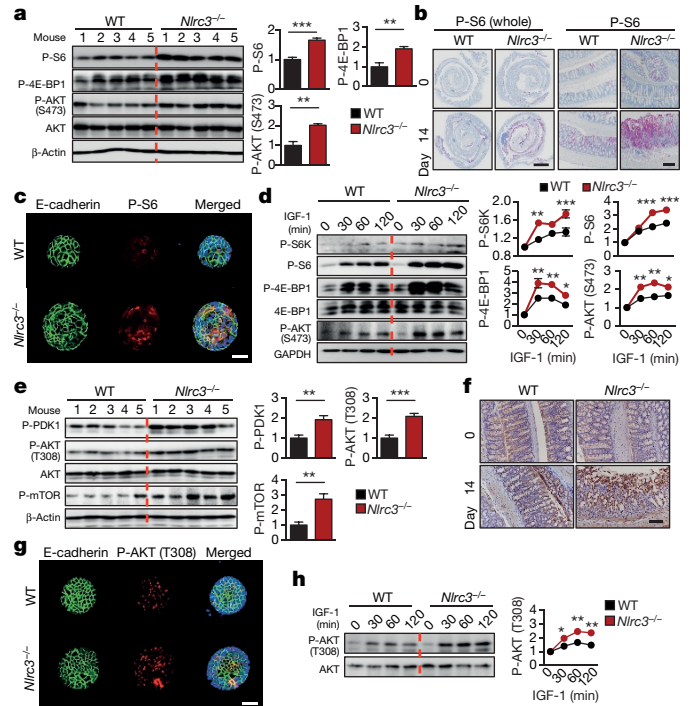


Figure 3 | NLRC3 controls mTOR signalling pathways. **a**, Immunoblot of mouse colon tissue and densitometric quantification at day 14. P- indicates phosphorylated protein. **b**, Immunohistochemical staining of mouse colon tissue. **c**, Immunofluorescence staining of mouse intestinal organoids after 7 days of culture. **d**, Immunoblot of organoids treated with IGF-1 and densitometric quantification. **e**, Immunoblot of colon tissue of mice and densitometric quantification at day 14. **f**, Immunohistochemical staining of colon tissue of mice for AKT that has been phosphorylated at Ser473. **g**, Immunofluorescence staining of mouse intestinal organoids after 7 days of culture. **h**, Immunoblot of organoids treated with IGF-1 and densitometric quantification. Scale bars, 2,500 μm (**b**, whole colon, left), 200 μm (**b**, magnified, right), 50 μm (**c**, **f**, **g**). **P* < 0.05; ***P* < 0.01; ****P* < 0.001; by two-tailed *t*-test (**a** and **e**) or one-way ANOVA (**d**, **h**). Data are from one experiment representative of two (**a–c**, **e–g**) or three independent experiments (**d**, **h**) and are presented as mean ± s.e.m. in **a**, **d**, **e** and **h**. For gel source data, see Supplementary Fig. 1.

elevated levels of many pro-inflammatory mediators at day 14, we observed increased levels of IκBα and STAT3 phosphorylation in the colon tissue of *Nlrc3*^{-/-} mice compared to wild-type mice (Extended Data Fig. 3b). However, differential phosphorylation of ERK was not observed (Extended Data Fig. 3b). Global increases in the production of inflammatory mediators and the activation of immune signalling pathways reflected the hyper-susceptibility of *Nlrc3*^{-/-} mice to colitis.

Using flow cytometry, we profiled the immune cell populations in the colons of untreated wild-type and *Nlrc3*^{-/-} mice and wild-type and *Nlrc3*^{-/-} mice at days 8 and 14. We observed an increased number of macrophages, neutrophils and natural killer cells in the colons of *Nlrc3*^{-/-} mice compared to wild-type mice 14 days after azoxymethane and DSS treatment (Extended Data Fig. 3c, d), which is consistent with the increased levels of inflammation observed at this time point. However, we did not observe differences in the relative number of macrophages, CD11b⁺CD11c⁺ cells, neutrophils, B cells, CD4⁺ T cells, CD8⁺ T cells and natural killer cells between untreated wild-type and *Nlrc3*^{-/-} mice or mice at day 8 (Extended Data Fig. 3d). NLRC3 has been implicated in the regulation of T-cell activation¹¹, however, we did not observe a difference in the levels of IFNγ⁺ or TNF⁺ CD4⁺ T cells when wild-type and *Nlrc3*^{-/-} splenocytes were stimulated with CD3 and CD28 in the presence of IL-2 (Extended Data Fig. 3e).

We performed bone-marrow chimaera studies to identify the contribution of NLRC3 in haematopoietic cells versus radioresistant stromal

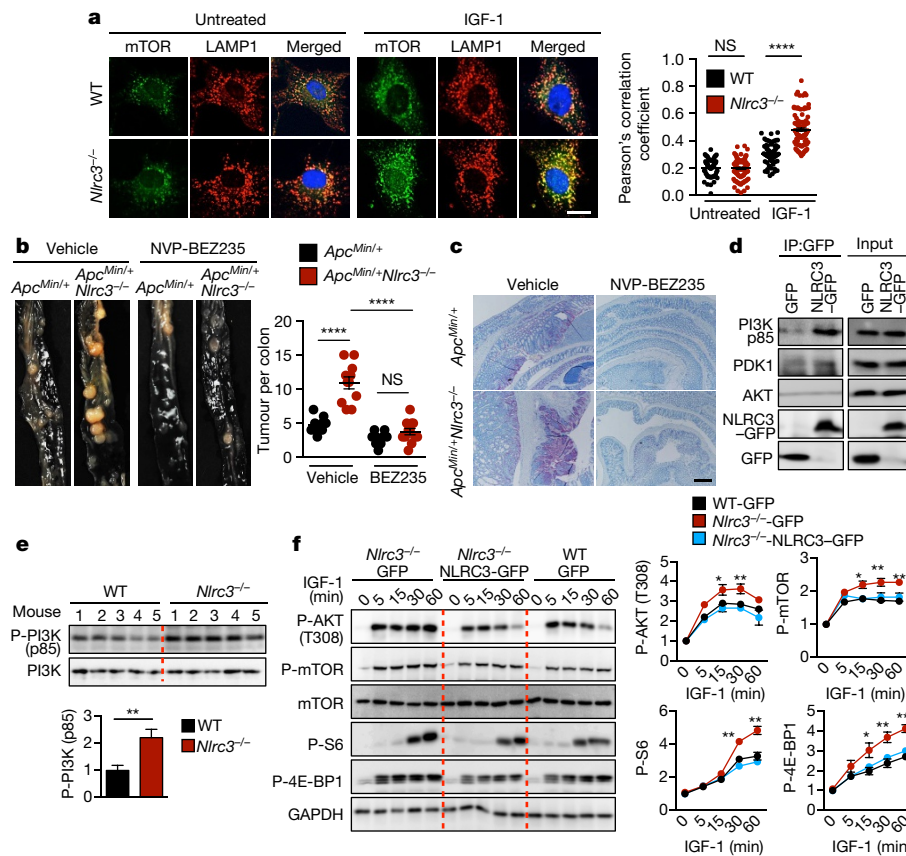


Figure 4 | NLRC3 regulates upstream signalling molecules within the PI3K–AKT–mTOR pathway. **a**, Immunofluorescence staining of primary fibroblasts and frequency of co-localization between mTOR and LAMP1 ($n \geq 150$). **b**, Images and quantification of colon tumours in littermate $Apc^{Min/+}$ and $Apc^{Min/+}Nlrc3^{-/-}$ mice 40 days after treatment with vehicle or NVP-BE2325. **c**, Immunohistochemical staining for phosphorylated S6 of colon tissue from mice treated as in **b**. **d**, Immunoprecipitation of the GFP tag in 239T cells transfected with a plasmid encoding GFP alone or NLRC3–GFP. **e**, Immunoblot of mouse colon tissue and densitometric

quantification at day 14. **f**, Immunoblot of primary mouse fibroblasts transfected with a retroviral vector encoding GFP or NLRC3–GFP, with or without stimulation with IGF-1, and densitometric quantification. Scale bar, 10 μm (**a**), 200 μm (**c**). * $P < 0.05$; ** $P < 0.01$; **** $P < 0.0001$; NS, no statistical significance by two tailed t -test (**e**) or one-way ANOVA (**a**, **b**, **f**). Data are from one experiment representative of two (**a**–**c**, **e**) or three (**d** and **f**) independent experiments (mean \pm s.e.m. in **a**, **b**, **e**, **f**). For gel source data, see Supplementary Fig. 1.

cells during colitis-associated tumorigenesis. As we expected, $Nlrc3^{-/-}$ mice that received $Nlrc3^{-/-}$ bone marrow were more susceptible to tumorigenesis than wild-type mice that received wild-type bone marrow (Fig. 1h and Extended Data Fig. 4a). However, $Nlrc3^{-/-}$ mice that received wild-type bone marrow had a significantly increased tumour burden compared with wild-type mice that received wild-type bone marrow. In addition, wild-type mice that received $Nlrc3^{-/-}$ bone marrow had a significantly increased tumour burden compared to wild-type mice that received wild-type bone marrow (Fig. 1h and Extended Data Fig. 4a). We further confirmed our findings and generated mice that lacked NLRC3 in haematopoietic cells specifically ($Vav1^{cre}Nlrc3^{fl/fl}$), cells of the myeloid lineage ($LysM^{cre}Nlrc3^{fl/fl}$) and intestinal epithelial cells ($Vil1^{cre}Nlrc3^{fl/fl}$). Mice lacking NLRC3 in intestinal epithelial cells developed the highest number of tumours, followed by mice lacking NLRC3 in haematopoietic cells (Fig. 1i and Extended Data Fig. 4b). Mice lacking NLRC3 in cells of the myeloid lineage had a similar number of tumours to wild-type mice (Fig. 1i and Extended Data Fig. 4b). These data support the observation that the oncogenic inhibitory effect of NLRC3 is more dominant in intestinal epithelial cells and more subtle in haematopoietic cells.

A closer examination of the intestinal epithelial cells of $Nlrc3^{-/-}$ mice revealed a significant increase in numbers of both Ki67⁺ and PCNA⁺ (both proteins that are associated with cellular proliferation) cells per intestinal crypt compared to wild-type mice at day 14 (Fig. 2a). Additionally, colonic epithelial stem cells collected from $Nlrc3^{-/-}$ mice more readily developed into organoids in *ex vivo* culture compared to

those collected from wild-type mice (Fig. 2b). The average diameters of the organoids derived from $Nlrc3^{-/-}$ mice were significantly increased compared to the average diameters of the organoids from wild-type mice (Fig. 2b). Expression of the stem-cell marker *Lgr5* in the colon tissue was similar in wild-type and $Nlrc3^{-/-}$ mice (Extended Data Fig. 4c), suggesting that the differences in the number and size of intestinal organoids was due to differential colony-forming capacity rather than differences in the numbers of starting intestinal stem cells. To investigate the effect of NLRC3 on cell proliferation more directly, we overexpressed NLRC3 in the human colon cell line HCT116 and found that these cells exhibited reduced levels of proliferation compared to cells expressing a control (GFP) protein (Fig. 2c). Furthermore, primary $Nlrc3^{-/-}$ fibroblasts proliferated more rapidly than wild-type fibroblasts (Fig. 2d).

Cellular proliferation can also be achieved when growth factors, nutrients and cellular energy activate metabolic pathways via the kinase mTOR¹⁶. We found increased phosphorylation levels of S6 kinase, 4E-BP1 and AKT at Ser473, the downstream targets of mTOR, in the colon tissue of $Nlrc3^{-/-}$ mice compared to wild-type mice at day 14 (Fig. 3a, b). Increased phosphorylation of these mTOR targets was also observed in $Nlrc3^{-/-}$ organoids compared to wild-type organoids (Fig. 3c, d). However, we found no difference in the expression of genes involved in the Wnt signalling pathway, including *Wnt1*, *Ctnnb1*, *Lef1*, *Tcf4*, *Tcf7* and *Axin2* (Extended Data Fig. 4c). The extent of nuclear localization of β -catenin was also similar between wild-type and $Nlrc3^{-/-}$ mice (Extended Data Fig. 4d).

Dysregulation of the mTOR signalling pathways in *Nlrc3*^{-/-} mice occurred very early, 8 days after injection of azoxymethane, whereas no difference in the production of inflammatory cytokines and mediators and phosphorylation of I κ B α was observed at this time point (Extended Data Fig. 5, a–c). Moreover, the differential AKT–mTOR signalling observed at this time point was not caused by differences in the relative levels of immune cells recruited to the colon (Extended Data Fig. 3d). These data suggest that the dysregulated mTOR signalling observed at an earlier time point may lead to increased NF- κ B signalling at a later time point.

Phosphorylation and activation of mTOR is driven by a number of upstream signalling proteins in the PI3K–AKT–mTOR pathway. Phosphorylation of AKT at the Thr308 site by the kinase PDK1 allows AKT to activate mTOR^{17–19}. To examine whether NLRC3 directly affects the apical molecules in the PI3K–AKT–mTOR pathway, we first investigated the phosphorylation status of AKT at the Thr308 site. We observed elevated phosphorylation of AKT at Thr308 in the colon tissue of *Nlrc3*^{-/-} mice compared to wild-type mice at day 14 (Fig. 3e). Increased levels of AKT phosphorylation in colon tissue were observed predominantly in epithelial cells and, to a lesser extent, in infiltrating cells (Fig. 3f). Similarly, increased phosphorylation of AKT at Thr308 was observed in *Nlrc3*^{-/-} organoids treated with IGF-1 compared to wild-type controls (Fig. 3g, h). We further observed increased activation of PDK1 in the colon tissue of *Nlrc3*^{-/-} mice treated with azoxymethane and DSS compared to wild-type mice (Fig. 3e). In addition, elevated degree of phosphorylation of AKT at Thr308 and of 4E-BP1 were observed in the colon of *Nlrc3*^{+/-} heterozygous mice compared to littermate wild-type mice at day 14, although this increase was smaller than that observed in littermate *Nlrc3*^{-/-} homozygous mice (Extended Data Fig. 6a). The gene-dose-dependent effect of NLRC3 on the suppression of the mTOR signalling pathways is reminiscent of the gene-dose-dependent effect of NLRC3 on the suppression of tumorigenesis (Fig. 1g).

Activated mTOR is phosphorylated and migrates to lysosomal and late endosomal membranes^{20,21}. We observed increased phosphorylation of mTOR in the colon tissue of *Nlrc3*^{-/-} mice (Fig. 3e). We also found an increased co-localization frequency between mTOR and LAMP1 puncta in IGF-1-treated primary *Nlrc3*^{-/-} fibroblasts compared to IGF-1-treated primary wild-type fibroblasts (Fig. 4a). Increased mTOR signalling was observed in *Nlrc3*^{-/-} fibroblasts or wild-type fibroblasts treated with short interfering RNAs (siRNAs) against *Nlrc3* compared to their corresponding controls (Extended Data Figs 6b–e, 7a–d).

We further investigated whether NLRC3 is able to restrict proliferation in a spontaneous mouse model of colon cancer. We crossed the mouse line containing a heterozygous mutation in the gene encoding adenomatous polyposis coli (*Apc*^{Min/+}) with *Nlrc3*^{-/-} mice and found that *Apc*^{Min/+}*Nlrc3*^{-/-} mice had a higher tumour burden than *Apc*^{Min/+} control mice (Extended Data Fig. 8a). Of the *Apc*^{Min/+}*Nlrc3*^{-/-} mice, 40% developed hyperplasia (compared to 0% in the littermate control group) and *Apc*^{Min/+}*Nlrc3*^{-/-} mice exhibited increased damage in the colon (Extended Data Fig. 8b, c). Notably, we observed increased number of Ki67⁺ proliferative cells and cells positive for phosphorylated S6 kinase in the colon of *Apc*^{Min/+}*Nlrc3*^{-/-} mice compared to *Apc*^{Min/+} mice (Extended Data Fig. 8c). Moreover, the capacity of *Apc*^{Min/+}*Nlrc3*^{-/-} intestinal stem cells to proliferate into organoids was greater than that of *Apc*^{Min/+} intestinal stem cells (Extended Data Fig. 8d). Treatment with the PI3K inhibitor LY294002 and the mTOR inhibitor rapamycin impaired the ability of intestinal stem cells to proliferate into organoids in both strains (Extended Data Fig. 8d). Treatment of the *Apc*^{Min/+} mice and *Apc*^{Min/+}*Nlrc3*^{-/-} mice with the PI3K–mTOR inhibitor NVP-BEZ235 reduced the tumour burden and phosphorylation of S6 kinase in the tumours and enterocytes of *Apc*^{Min/+}*Nlrc3*^{-/-} mice to a level observed in treated *Apc*^{Min/+} mice (Fig. 4b, c). Collectively, these data suggest that NLRC3 restricts cellular proliferation via the PI3K–mTOR axis during colon tumorigenesis.

Following generation of inositol phospholipids by activated PI3Ks, AKT is recruited to the cell membrane where it undergoes a conformational change and is phosphorylated at Thr308 by PDK1 (refs 17–19). Co-immunoprecipitation assays showed that NLRC3 weakly interacted with PDK1 and did not interact with AKT (Fig. 4d). Instead, we found that NLRC3 co-immunoprecipitated with p85 subunits of PI3K (Fig. 4d). In addition, we observed increased levels of interaction between the p85 and p110 α subunits of PI3K in *Nlrc3*^{-/-} primary fibroblasts or mouse bone-marrow-derived macrophages (BMDMs) (Extended Data Fig. 9a, b). We also observed a higher level of phosphorylation and activation of p85 PI3K in the colon tissue of *Nlrc3*^{-/-} mice treated with azoxymethane and DSS compared to wild-type mice (Fig. 4e). These data provide evidence to suggest that NLRC3 disrupts an association between the PI3K p85 and p110 α subunits and reduces the activity of PI3K p85 itself. Deletion of the CARD, NACHT or LRR domain of NLRC3 impaired the ability of NLRC3 to interact with either the p85 or the p110 α subunit of PI3K (Extended Data Fig. 9c–g). Reconstitution of NLRC3 in *Nlrc3*^{-/-} fibroblasts reduced the degree of phosphorylation of AKT Thr308 and other downstream molecules to levels similar to those seen in wild-type fibroblasts upon stimulation with IGF-1 (Fig. 4f).

In addition to growth factor receptors, activation of TLR4 can engage the PI3K–AKT–mTOR pathway^{22–24}. We observed increased activation of the mTOR signalling pathways in lipopolysaccharide (LPS)-treated primary *Nlrc3*^{-/-} BMDMs compared to LPS-treated wild-type BMDMs (Extended Data Fig. 10a, b). We further confirmed our findings in an independently generated line of NLRC3-deficient mice that we term *Nlrc3*^{3/d/d} mice (NLRC3 large deletion, data not shown; see Methods). Collectively these findings identify NLRC3 as an inhibitory sensor of the PI3K–AKT–mTOR pathway, mediating protection against tumorigenesis in colorectal cancer (Extended Data Fig. 10c).

NLRC3 does not act solely to protect against cancer. A previous study has shown that expression of NLRC3 is downregulated in patients with the autoimmune disease Wegener's granulomatosis²⁵. Moreover, a loss-of-function mutation in the gene encoding the NLRC3-like protein in zebrafish results in systemic inflammation²⁶. These findings collectively provide evidence to support the cross-species functionality of NLRC3. Whether NLRC3 needs to be bound to a specific ligand or is engaged in the activation of its regulatory function in a ligand-independent manner remains to be explored. Understanding the precise functions of NLRC3 could open up new avenues in the treatment of infectious and autoinflammatory diseases and cancer.

Online Content Methods, along with any additional Extended Data display items and Source Data, are available in the online version of the paper; references unique to these sections appear only in the online paper.

Received 18 November 2015; accepted 2 November 2016.

Published online 12 December 2016.

1. Ting, J. P., Willingham, S. B. & Bergstralh, D. T. NLRs at the intersection of cell death and immunity. *Nat. Rev. Immunol.* **8**, 372–379 (2008).
2. Zaki, M. H. et al. The NLRP3 inflammasome protects against loss of epithelial integrity and mortality during experimental colitis. *Immunity* **32**, 379–391 (2010).
3. Zaki, M. H., Vogel, P., Body-Malapel, M., Lamkanfi, M. & Kanneganti, T. D. IL-18 production downstream of the Nlrp3 inflammasome confers protection against colorectal tumor formation. *J. Immunol.* **185**, 4912–4920 (2010).
4. Allen, I. C. et al. The NLRP3 inflammasome functions as a negative regulator of tumorigenesis during colitis-associated cancer. *J. Exp. Med.* **207**, 1045–1056 (2010).
5. Allen, I. C. et al. NLRP12 suppresses colon inflammation and tumorigenesis through the negative regulation of noncanonical NF- κ B signaling. *Immunity* **36**, 742–754 (2012).
6. Elinav, E. et al. NLRP6 inflammasome regulates colonic microbial ecology and risk for colitis. *Cell* **145**, 745–757 (2011).
7. Man, S. M. et al. Critical role for the DNA sensor AIM2 in stem cell proliferation and cancer. *Cell* **162**, 45–58 (2015).
8. Wilson, J. E. et al. Inflammasome-independent role of AIM2 in suppressing colon tumorigenesis via DNA-PK and Akt. *Nat. Med.* **21**, 906–913 (2015).
9. Zaki, M. H. et al. The NOD-like receptor NLRP12 attenuates colon inflammation and tumorigenesis. *Cancer Cell* **20**, 649–660 (2011).

10. Harton, J. A., Linhoff, M. W., Zhang, J. & Ting, J. P. Cutting edge: CATERPILLER: a large family of mammalian genes containing CARD, pyrin, nucleotide-binding, and leucine-rich repeat domains. *J. Immunol.* **169**, 4088–4093 (2002).
11. Conti, B. J. *et al.* CATERPILLER 16.2 (CLR16.2), a novel NBD/LRR family member that negatively regulates T cell function. *J. Biol. Chem.* **280**, 18375–18385 (2005).
12. Liu, R. *et al.* Expression profile of innate immune receptors, NLRs and AIM2, in human colorectal cancer: correlation with cancer stages and inflammasome components. *Oncotarget* **6**, 33456–33469 (2015).
13. Schneider, M. *et al.* The innate immune sensor NLRC3 attenuates Toll-like receptor signaling via modification of the signaling adaptor TRAF6 and transcription factor NF- κ B. *Nat. Immunol.* **13**, 823–831 (2012).
14. Zhang, L. *et al.* NLRC3, a member of the NLR family of proteins, is a negative regulator of innate immune signaling induced by the DNA sensor STING. *Immunity* **40**, 329–341 (2014).
15. Man, S. M. & Kanneganti, T. D. Converging roles of caspases in inflammasome activation, cell death and innate immunity. *Nat. Rev. Immunol.* **16**, 7–21 (2016).
16. Shimobayashi, M. & Hall, M. N. Making new contacts: the mTOR network in metabolism and signalling crosstalk. *Nat. Rev. Mol. Cell Biol.* **15**, 155–162 (2014).
17. Alessi, D. R. *et al.* Characterization of a 3-phosphoinositide-dependent protein kinase which phosphorylates and activates protein kinase B α . *Curr. Biol.* **7**, 261–269 (1997).
18. Stephens, L. *et al.* Protein kinase B kinases that mediate phosphatidylinositol 3,4,5-trisphosphate-dependent activation of protein kinase B. *Science* **279**, 710–714 (1998).
19. Stokoe, D. *et al.* Dual role of phosphatidylinositol-3,4,5-trisphosphate in the activation of protein kinase B. *Science* **277**, 567–570 (1997).
20. Sancak, Y. *et al.* Ragulator–Rag complex targets mTORC1 to the lysosomal surface and is necessary for its activation by amino acids. *Cell* **141**, 290–303 (2010).
21. Zoncu, R. *et al.* mTORC1 senses lysosomal amino acids through an inside-out mechanism that requires the vacuolar H⁺-ATPase. *Science* **334**, 678–683 (2011).
22. Monick, M. M. *et al.* Lipopolysaccharide activates Akt in human alveolar macrophages resulting in nuclear accumulation and transcriptional activity of β -catenin. *J. Immunol.* **166**, 4713–4720 (2001).
23. Jones, B. W., Heldwein, K. A., Means, T. K., Saukkonen, J. J. & Fenton, M. J. Differential roles of Toll-like receptors in the elicitation of proinflammatory responses by macrophages. *Ann. Rheum. Dis.* **60** (Suppl. 3), iii6–iii12 (2001).
24. Ojaniemi, M. *et al.* Phosphatidylinositol 3-kinase is involved in Toll-like receptor 4-mediated cytokine expression in mouse macrophages. *Eur. J. Immunol.* **33**, 597–605 (2003).
25. Laudien, M. *et al.* Molecular signatures of a disturbed nasal barrier function in the primary tissue of Wegener's granulomatosis. *Mucosal Immunol.* **4**, 564–573 (2011).
26. Shiau, C. E., Monk, K. R., Joo, W. & Talbot, W. S. An anti-inflammatory NOD-like receptor is required for microglia development. *Cell Reports* **5**, 1342–1352 (2013).

Supplementary Information is available in the online version of the paper.

Acknowledgements We thank the Transgenic Gene Knockout Shared Resource at St. Jude Children's Research Hospital (SJCRH) for assistance with knockout mouse generation. Images were acquired at the SJCRH Cell & Tissue Imaging Center, which is supported by SJCRH and NCI grant P30 CA021765-35. Work from our laboratory is supported by the US National Institutes of Health (grants AI101935, AI124346, ARO56296 and CA163507 to T.-D.K.), ALSAC (to T.-D.K.), and the ExC306 Inflammation at Interfaces, the DFG SFB 877 B9 and DFG SFB1182 C2 projects (to P.R.). S.M.M. is supported by the R. G. Menzies Early Career Fellowship from the National Health and Medical Research Council of Australia.

Author Contributions R.K., S.M.M. and T.-D.K. conceptualized the study; R.K., S.M.M., R.K.S.M. and S.K. designed the methodology; R.K., S.M.M., R.K.S.M., S.K., Q.Z., B.R.S., A.R.B., X.Q., S.P. and P.V. performed the experiments; R.K., S.M.M., R.K.S.M., S.K., Q.Z. and P.V. conducted the analysis; R.K., S.M.M. and T.-D.K. wrote the manuscript; P.R. and T.-D.K. provided resources; T.-D.K. provided overall supervision.

Author Information Reprints and permissions information is available at www.nature.com/reprints. The authors declare no competing financial interests. Readers are welcome to comment on the online version of the paper. Correspondence and requests for materials should be addressed to T.-D.K. (thirumala-devi.kanneganti@stjude.org).

METHODS

Mice. Wild-type (C57BL/6) and *Nlr3*^{-/-} mice were bred and maintained under specific pathogen-free conditions at St. Jude Children's Research Hospital. To generate the *Nlr3*^{-/-} mice, exons 2 and 3 of the gene encoding NLR3 (2.5 kb) were excised, which resulted in deletion of 661 amino acids encoding the N-terminal caspase-recruitment domain (also known as CARD) and the central nucleotide-binding domain (also known as NACHT) of NLR3. Splicing of exon 1 and exon 4 led to a frameshift, generating a premature stop codon (Extended Data Fig. 1c). The targeting vector ROS1-HR was linearized and transfected into embryonic stem (ES) cells. Cells positive for the targeting vector were selected by resistance to 200 µg ml⁻¹ of G418 and further screened for 5' and 3' homologous recombination. ES cell clones with the correct targeting events were used for blastocysts injection. CMV-Cre mice were used to delete the conditional floxed *Nlr3* allele to generate the *Nlr3*^{-/-} mice. B6.129P2-*Lyz2*^{tm1(cre)Jfo/J} (004781, The Jackson Laboratory), B6.Cg-Tg(Vav1-cre)A2Kio/J (008610, The Jackson Laboratory) and B6.Cg-Tg(Vil-cre)997Gum/J mice (004586, The Jackson Laboratory) were used to delete the conditional floxed *Nlr3* allele in a cell-type-specific manner. Expression of NLR3 in wild-type and *Nlr3*^{-/-} mice were confirmed by genomic PCR amplification (Extended Data Fig. 1c). *Nlr3*^{-/-} mice were backcrossed to C57BL/6 for nine generations.

Nlr3^{3'del} (*Nlr3* large deletion) mice were generated by injection of two single guide RNAs (Nlr3-Guide-01: 3'-ATCCAGGTCGCTCTAGGC-5'; 125 ng µl⁻¹) and Nlr3-Guide-02: 3'-AGTGAACAGCACAGTTCGC-5'; 125 ng µl⁻¹), designed to introduce DNA double-strand breaks into intron 1 and intron 3 of the *Nlr3* gene, together with a codon-optimized Cas9 mRNA transcript (50 ng µl⁻¹) into the cytoplasm of the pronuclear stage C57BL/6J zygotes (Transgenic Core Unit, St. Jude Children's Research Hospital). Injected embryos were surgically transplanted into oviducts of pseudo pregnant CD1 females and new-born mice bearing the intron-1-to-intron-3 deletion (~3.8 kb) were identified by the amplification of a 1.1-kb fragment using primers flanking the two break sites: Nlr3-F51: 3'-AGAGTGGTGCCATCTCTGC-5' and Nlr3-R32: 3'-CTCAAGTCAGGGCAGCATGA-5'. Sanger sequencing of the ~1.1-kb amplicon confirmed proper deletion of the 3.8-kb fragment containing exon 2 and 3. The sgRNAs and Cas9 mRNA transcript were designed and generated as described previously²⁷. Potential off-target sites were identified using Cas-OFFinder²⁸, amplified by PCR and sequenced. No off-target site cleavage was observed. Two founder mice were used to establish the mouse lines. Animal study protocols were approved by the St. Jude Children's Research Hospital Committee on Use and Care of Animals.

Azoxymethane-DSS model of colorectal tumorigenesis. Male and female mice were used at the age of six weeks. For cohousing experiments, wild-type and *Nlr3*^{-/-} mice were co-housed for three weeks and separated before injection of azoxymethane. We also performed experiments whereby wild-type and *Nlr3*^{-/-} mice were co-housed for three weeks before injection of azoxymethane and remained co-housed over the course of the experiments. In both cases, the results did not differ. Mice were injected intraperitoneally with 10 mg of azoxymethane (A5486, Sigma) per kg body weight, according to previously established protocols^{7,29}. After 5 days, 2% DSS (9011-18-1, Affymetrix eBioscience) was given in the drinking water for 6 days followed by regular drinking water for 2 weeks. This cycle was repeated twice more with 1.5% DSS and mice were killed on day 80 (Extended Data Fig. 1a). For day 8 samples, mice were injected with azoxymethane, and after 5 days, fed with 2% DSS for 3 days before being killed. For Day 14 samples, mice were injected with azoxymethane, and after 5 days, fed with 2% DSS for 6 days. Mice were then fed with regular water for 3 days and collected. Bone-marrow chimera studies were performed as described previously⁷. No randomization or blinding was performed.

***Apc*^{Min} model of colorectal tumorigenesis.** C57BL/6J-*Apc*^{Min/+} mice (002020, The Jackson Laboratory) were crossed with *Nlr3*^{-/-} mice. Littermate *Apc*^{Min/+} and *Apc*^{Min/+} *Nlr3*^{-/-} mice were administered with either 40 mg kg⁻¹ body weight of the dual inhibitor of PI3K and mTOR, NVP-BE235 (N-4288, LC Laboratories) dissolved in 10% (v/v) 1-methyl-2-pyrrolidone (328634, Sigma) plus 90% (v/v) polyethylene glycol 300 (90878, Sigma) or the control vehicle 10% (v/v) 1-methyl-2-pyrrolidone plus 90% (v/v) polyethylene glycol 300 by daily oral gavage for 40 days from 6 weeks of age.

Histology and microscopy analysis. Colons were rolled into a 'Swiss roll' and fixed in 10% formalin, processed and embedded in paraffin by standard techniques. Longitudinal sections of 5 µm were stained with haematoxylin and eosin and examined by a pathologist blinded to the experimental groups. Colitis scores were assigned based on inflammation, ulceration, hyperplasia and the extent or severity of damage. Severity scores for inflammation were assigned as follows: 0 = normal (within normal limits); 2 = minimal (mixed inflammation, small, focal or widely separated, limited to lamina propria); 15 = mild (multifocal mixed inflammation, often extending into submucosa); 40 = moderate (large multifocal lesions within

mixed inflammation involving mucosa and submucosa); 80 = marked (extensive mixed inflammation with oedema and erosions); 100 = severe (diffuse inflammation with transmural lesions and multiple ulcers). Scores for ulceration were assigned as follows: 0 = normal (none); 2 = minimal (only one small focus of ulceration involving fewer than 5 crypts); 15 = mild (a few small ulcers up to 5 crypts); 40 = moderate (multifocal ulcers up to 10 crypts); 80 = marked (multifocal to coalescing ulcers involving more than 10 crypts each); 100 = severe (extensive to diffuse with multiple ulcers covering more than 20 crypts each). Scores of hyperplasia were assigned as follows: 0 = normal; 2 = minimal (some areas with crypts elongated and increased mitoses); 15 = mild (multifocal areas with crypts elongated up to twice the normal thickness, normal goblet cells present); 40 = moderate (extensive areas with crypts up to twice the normal thickness, reduced goblet cells); 80 = marked (mucosa over twice the normal thickness, hyperchromatic epithelium, reduced or rare goblet cells, possibly foci of arborization); 100 = severe (mucosa twice the normal thickness, marked hyperchromasia, crowding or stacking, absence of goblet cells, high mitotic index and arborization). Scores of extent were assigned as follows: 0 = normal (rare or inconspicuous lesions); 2 = minimal (less than 5% involvement); 15 = mild (multifocal but conspicuous lesions, 5–10% involvement); 40 = moderate (multifocal, prominent lesions, 10–50% involvement); 80 = marked (coalescing to extensive lesions or areas of inflammation with some loss of structure, 50–90% involvement); 100 = severe (diffuse lesion with effacement of normal structure, over 90% involvement). The proliferating cells in the intestinal epithelium were detected by immunoperoxidase staining for Ki67 and PCNA. The immunohistochemistry antibodies used were: Ki67 (NBPI-40684, Novus), PCNA (M0879, DAKO), β-catenin (610154, BD), P-AKT Ser473 (4060, Cell Signaling), and P-S6 Ribosomal Protein Ser235-236 (4858, Cell Signaling). Tissues were counterstained with haematoxylin. The number of Ki67⁺ or PCNA⁺ cells per crypt in each animal was counted (at least 18–20 crypts per mouse).

Cell culture and stimulation of cells. Pinna of adult wild-type and *Nlr3*^{-/-} mice were minced and digested with 100 mg ml⁻¹ collagenase type IV (LS004188, Worthington Biochemical Corporation) for 3 h, followed by filtration through 70-µm strainers to obtain fibroblasts. Cells were cultured in 50% FBS (TMS-013-B, Millipore) in DMEM (11995073, ThermoFisher Scientific) supplemented with HEPES (15630-080, ThermoFisher Scientific), 1% penicillin and streptomycin (15070-063, ThermoFisher Scientific), L-glutamine (25030, ThermoFisher Scientific), sodium pyruvate (11360, ThermoFisher Scientific), non-essential amino acids (11140, ThermoFisher Scientific), and β-mercaptoethanol (21985023, ThermoFisher Scientific) for the first 3–4 days. Cells were subcultured in DMEM supplemented with 10% FBS and 1% penicillin and streptomycin. All primary fibroblasts were used before reaching the sixth passage. Fibroblasts were seeded onto six-well plates at a density of 2 × 10⁵ cells per well. Cells were deprived of serum for 36 h and further incubated in PBS for 1 h. Cells were then stimulated with 50 ng ml⁻¹ of recombinant murine IGF-1 (250-19, Peprotech) for the indicated time.

BMDMs were cultured as described previously³⁰. BMDMs were stimulated with 500 ng ml⁻¹ ultrapure LPS from *Salmonella minnesota* R595 (trl-smlps, InvivoGen) for the indicated time. The human colorectal carcinoma HCT116 cell line (ATCC#CCL-247, American Type Culture Collection) was cultured in McCoy's 5A medium (16600-082, ThermoFisher Scientific) supplemented with 10% FBS and 1% penicillin and streptomycin. The embryonic kidney epithelial cell line HEK293T (ATCC#3216, American Type Culture Collection) and L929 cell line (ATCC#CRL-2648, American Type Culture Collection) were cultured in DMEM supplemented with 10% FBS. All cell lines were maintained at 37 °C with 5% CO₂.

Colon organoid culture. Mouse colon stem cells were cultured using IntestiCult organoid growth medium according to the manufacturer's instructions (06005, STEMCELL Technologies). The whole colon was removed from untreated wild-type and *Nlr3*^{-/-} mice and rinsed with cold PBS. The colon was cut into 2-mm segments and washed 20 times with cold PBS. Colonic segments were incubated in Gentle Cell Dissociation Reagent (07174, STEMCELL Technologies), rotated at 350g for 15 min at room temperature, followed by re-suspension in PBS supplemented with 0.1% BSA (A6003, Sigma). Dissociated colonic crypts were filtered through 70-µm strainers. Dissociated colonic crypts were resuspended in DMEM/F12 medium with 15 mM HEPES (36254, STEMCELL Technologies), counted and resuspended in Intesticult organoid growth medium and Matrigel (356230, Corning) in a 1:1 ratio. Cells were plated in 24-well culture plates (3738, Corning). Intesticult organoid growth medium were added to the cell culture plates to immerse the matrix composed of Intesticult organoid growth medium and Matrigel. For inhibition studies, 50 µM of LY294002 (440202, Millipore) or 10 µg ml⁻¹ rapamycin (553210, Sigma) was added to the Intesticult organoid growth medium.

Proliferation assay. Cell proliferation was measured using the WST-1 reagent (05015944001, Roche). Primary ear fibroblasts or HCT116 cells were plated at a density of 5,000 cells per well in 96-well tissue culture plates and incubated

overnight. Cells were deprived of serum for 36 h and exposed to normal culture media for the indicated time interval. The WST-1 reagent was added to the cells for 2 h. Plates were then read at 450 nm. The number of cells was calculated using a standard curve³¹.

Immunoblotting. Proteins were extracted from colon tissue or cells using RIPA lysis buffer supplemented with protease (11697498001, Roche) and phosphatase inhibitors (04906837001, Roche) as described previously³². Samples were resolved in 8–15% SDS–PAGE and transferred onto PVDF membranes (IPVH00010, Millipore). Blocking was performed in 5% milk for 1 h and membranes were incubated in primary antibodies overnight at 4 °C. Membranes were incubated with HRP-conjugated secondary antibody for 1 h and proteins were visualized using Super Signal Femto substrate (34096, ThermoFisher Scientific). The primary antibodies used were P-ERK (1:1,000, 9101, Cell Signaling), ERK (1:1,000, 9102, Cell Signaling), P-IκBα (1:1,000, 9241, Cell Signaling), IκBα (1:1,000, 9242, Cell Signaling), P-AKT Ser473 (1:1,000, 4060, Cell Signaling), P-AKT Thr308 (1:1,000, 13038), AKT (1:1,000, 4691, Cell Signaling), P-mTOR Ser2448 (1:1,000, 2971, Cell Signaling), mTOR (1:1,000, 2972, Cell Signaling), P-p70 S6K Thr389 (1:1,000, 9205, Cell Signaling), P-S6 Ser235/236 (1:1,000, 4856, Cell Signaling), P-4E-BP1 Thr37/46 (1:1,000, 2855, Cell Signaling), P-STAT3 Tyr705 (1:1,000, 9131, Cell Signaling), P-PDK1 (1:1,000, 3061, Cell Signaling), PDK1 (1:1,000, 3062, Cell Signaling), P-PI3K p85 (1:1,000, 4228, Cell Signaling), PI3K p85 (1:1,000, 4257, Cell Signaling), PI3K p110α (1:1,000, 4249, Cell Signaling), mouse anti-GFP (1:2,000, sc-9996, Santa Cruz Biotechnology), rabbit anti-GFP (1:2,000, sc-8334, Santa Cruz Biotechnology), β-actin (1:2,000, 8457, Cell Signaling), and anti-GAPDH (1:10,000, 5174, Cell Signaling). Immunoblots were quantified using ImageJ.

Immunofluorescence staining. Serum-deprived primary ear fibroblasts were left untreated or stimulated with IGF-1 for 30 min. Fibroblasts or six-day-old intestinal organoids were washed three times with PBS and were fixed for 15 min at room temperature in 4% paraformaldehyde, followed by blocking in 10% normal goat serum (X090710-8, Dako) supplemented with 0.1% saponin (47036, Sigma). Fibroblasts or organoids were incubated with the following antibodies overnight at 4 °C: P-AKT Ser473 (1:200, 4060, Cell Signaling), P-AKT Thr308 (1:200, 13038), P-S6 Ser235/236 (1:500, 4856, Cell Signaling), P-4E-BP1 Thr37/46 (1:200, 2855, Cell Signaling). Samples were also stained with Alexa Fluor 488 phalloidin (1:500, A12379, ThermoFisher Scientific) or Alexa Fluor 488 E-cadherin (1:200, 53-3249-80, Affymetrix eBioscience). To analyse mTOR activation, cells were incubated overnight at 4 °C with antibodies against mTOR (1:200, 2983, Cell Signaling) and LAMP1 (1:1,000, eBioD4B, Affymetrix eBioscience). The secondary antibodies used were Alexa Fluor 568-conjugated antibody to rabbit immunoglobulin G (1:250; A11036; ThermoFisher Scientific), Alexa Fluor 568-conjugated antibody to rat immunoglobulin G (1:250; A11077; ThermoFisher Scientific) and Alexa Fluor 488-conjugated antibody to rabbit immunoglobulin G (1:250; A11034; ThermoFisher Scientific). Cells and organoids were counterstained in DAPI mounting medium (H-1200, Vecta Labs) and images taken with a Nikon C2 confocal microscope. The average density unit and the Pearson's correlation coefficient were calculated using the digital microscopy imaging software SlideBook 5 (Intelligent Imaging Innovations).

Quantitative reverse-transcriptase PCR. RNA was isolated using TRIzol (15596026, ThermoFisher Scientific) and converted to cDNA using the High-Capacity cDNA Reverse Transcription kit (4368814, Applied Biosystems). Gene expression was assessed using the 2 × SYBR Green kit (4368706, Applied Biosystems) according to the manufacturer's instructions. Primer sequences are listed in the Supplementary Information.

Cytokine measurement by ELISA. Cytokines in the colon and sera were measured by ELISA according to manufacturer's instructions. IL-18 was measured using an ELISA kit (BMS618/3TEN, Affymetrix eBioscience) and all other cytokines were measured by a multiplex ELISAs (MICYTOMAG-70K, Millipore).

Flow cytometry. Colons were dissected, washed with ice-cold PBS and cut into small pieces. Colon pieces were incubated with PBS containing 1 mM DTT, 5 mM EDTA and 10 mM HEPES at 37 °C for 30 min with gentle shaking to remove the epithelial layer. The colon segments were further digested in RPMI medium containing 0.5 mg ml⁻¹ collagenase D at 37 °C for 1.5 h. The supernatant was passed through 70-μm cell strainer and enriched by 37.5% Percoll to isolate lamina propria cells.

The following monoclonal antibodies were used for flow cytometry: CD4 (RM4-5; 14-0042-85), CD11b (M1/70; 48-0112-82) and CD8a (53-6.7; 48-0081-82) from Affymetrix eBioscience, CD19 (6D5; 115512), NK1.1 (PK136; 108708), CD11c (N418; 117306), Gr1 (RB6-8C5; 108426) and F4/80 (BM8; 123109) from BioLegend. The dilution factor for all antibodies was 1:300. The following gating strategies were used: B cells were gated as live cells and CD19⁺. CD4⁺ T cells were gated as live cells, CD4⁺ and CD8⁻. CD8⁺ T cells were gated as live cells, CD8⁺ and CD4⁻. Natural killer cells were gated as live cells and NK1.1⁺. Macrophages were gated as live cells, CD11b⁺, Gr1^{low-neg}, F4/80⁺ and CD11c⁻. Neutrophils were gated as live cells, CD11b⁺ and Gr1^{hi}. CD11b⁺CD11c⁺ cells were gated as live cells,

CD11b⁺, Gr1^{low-neg}, CD11c⁺ and F4/80⁻. Flow cytometry data were acquired on a BD FACSCalibur and analysed using TreeStar FlowJo software.

T-cell stimulation and intracellular cytokine staining. Splenocytes from wild-type and *Nlr3*^{-/-} mice were treated with ACK lysis buffer at room temperature for 1 min to remove red blood cells. Splenocytes were washed, counted and plated at 2 × 10⁵ cells per well in a 96-well plate coated with 1 μg ml⁻¹ anti-CD3 (145-2C11, Affymetrix eBioscience) and 1 μg ml⁻¹ anti-CD28 (16-0281, Affymetrix eBioscience). Cells were cultured at 37 °C in the presence and absence of 20 ng ml⁻¹ murine IL-2 (212-12, Peprotech) for 4 days. Brefeldin A (00-4506, Affymetrix eBioscience) was added to the media for 3 h, followed by washing in PBS, and staining with anti-CD4 (14-0042-85, Affymetrix eBioscience) and anti-CD3 (145-2C11, Affymetrix eBioscience) antibodies on ice for 20 min. Stained cells were fixed in 1% paraformaldehyde for 30 min on ice and permeabilized using permeabilization buffer (00-8333-56, Affymetrix eBioscience) according to manufacturer's instructions. To detect intracellular cytokines, fixed cells were stained with anti-IFNγ (50-7311, Tonbo) and anti-TNF (506322, Biolegend) for 30 min on ice. Flow cytometry were performed as described above.

siRNA knockdown. Primary ear fibroblasts were transfected with a siRNA from siGENOME smart pools with the assistance of the Neon Transfection System (MPK5000, ThermoFisher Scientific). The siGENOME SMARTpool siRNA specific for the gene encoding mouse NLRC3 (M-052823-01, Dharmacon) and a control siRNA pool were used. Sequences for siRNA are listed in Supplementary Information. After 48 h of transfection, cells were stimulated with IGF-1 as described above.

Retroviral transduction. Human or mouse MSCV-NLRC3-IRES-GFP or MSCV-IRES-GFP construct was co-transfected with retroviral packaging plasmids (pPAM-E and VSV-G) into HEK293T cells using Xfect Transfection Reagents (631318, Clontech Laboratories, Inc.). Virus-containing media were collected 48–72 h later and passed through a 0.45-μm filter. Primary ear fibroblasts or HCT116 cells were transduced with control or NLRC3-encoding retroviral vectors. Cells expressing GFP were selected by flow cytometry.

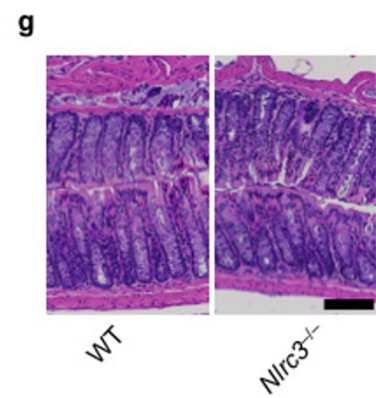
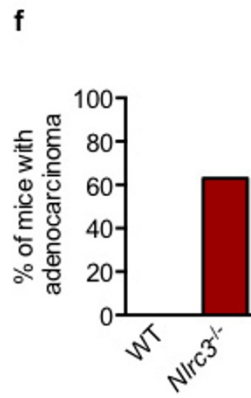
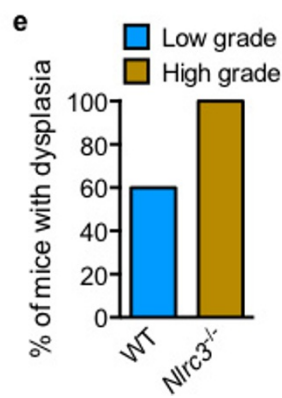
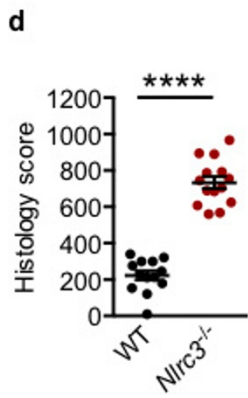
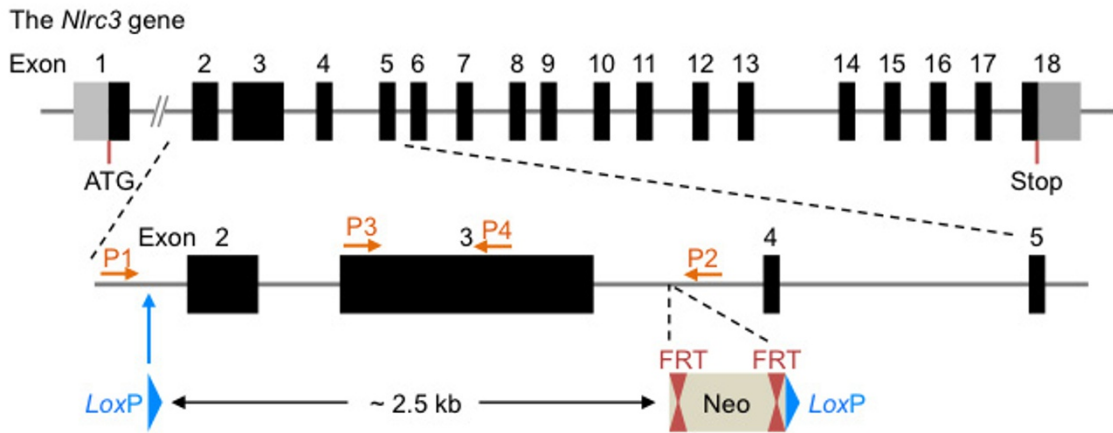
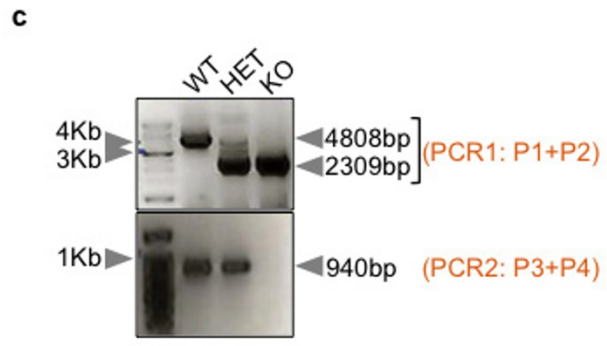
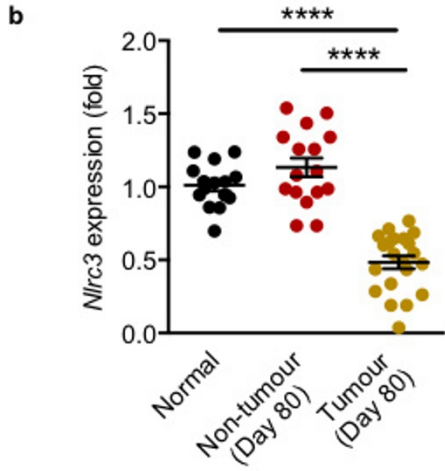
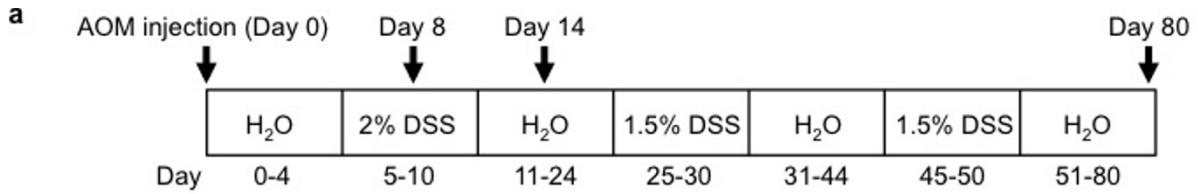
Generation of cells expressing NLRC3 and its deletion mutants. Plasmids pVSVg, pPAM-E and pMIGII encoding the mouse *Nlr3* gene or the mouse *Nlr3* gene lacking regions encoding the CARD, NACHT or LRR domain was transfected into L929 cells to generate retroviral stocks. Domains were annotated in accordance with the NCBI Conserved Domain (<http://www.ncbi.nlm.nih.gov/Structure/cdd/wrpsb.cgi>). Retroviral supernatants were collected after 48 h of transfection and filtered through 0.4-μm filters. L929 cells were infected with the retroviral stocks in the presence of polybrene to generate cells that stably expressed either wild-type NLRC3 or NLRC3 lacking regions encoding the CARD, NACHT or LRR domain.

Co-immunoprecipitation. Cells were collected with ice-cold PBS and lysed in lysis buffer composed of 50 mM Tris-HCl pH 7.5, 150 mM NaCl, 1% NP-40, protease and phosphatase inhibitors. Lysates were cleared of insoluble material by centrifugation at 15,000g for 10 min. For immunoprecipitation, cell lysates were incubated with 3 μg of primary antibodies at 4 °C for 12–16 h on a rocking platform, followed by incubation with Protein A/G PLUS-Agarose (sc-2003, Santa Cruz) for a further 2 h on a rocking platform. The immunoprecipitated products were washed three times with lysis buffer and eluted using 2 × SDS sample buffer and boiled at 100 °C for 5 min.

Statistical analysis. GraphPad Prism 6.0 software was used for data analysis. Data are shown as mean ± s.e.m. Statistical significance was determined by *t*-test (two-tailed) for two groups or one-way ANOVA (with multiple comparisons tests) for three or more groups. *P* < 0.05 was considered statistically significant. No statistical methods were used to predetermine sample size.

Data availability. Source data for Figs 3a, d, e, h, 4d–f and Extended Data Figs 3b, 5a, 6a, b, d, e, 9a, b, d–g, 10a, b have been provided in Supplementary Fig. 1. All other data supporting the findings of this study are available from the corresponding author on request.

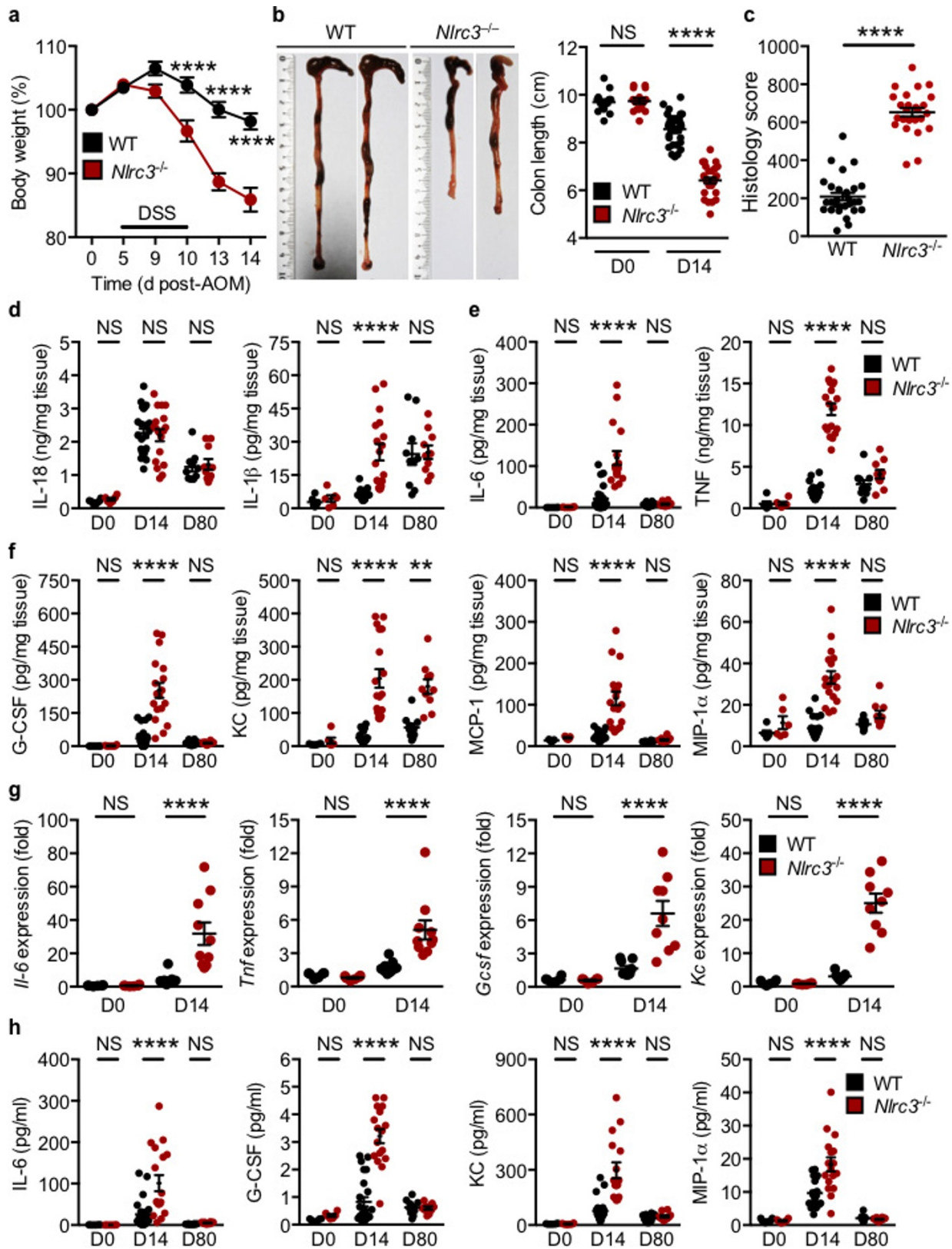
- Pelletier, S., Gingras, S. & Green, D. R. Mouse genome engineering via CRISPR-Cas9 for study of immune function. *Immunity* **42**, 18–27 (2015).
- Bae, S., Park, J. & Kim, J. S. Cas-OFFinder: a fast and versatile algorithm that searches for potential off-target sites of Cas9 RNA-guided endonucleases. *Bioinformatics* **30**, 1473–1475 (2014).
- Zhu, Q. *et al.* Cutting edge: STING mediates protection against colorectal tumorigenesis by governing the magnitude of intestinal inflammation. *J. Immunol.* **193**, 4779–4782 (2014).
- Man, S. M. *et al.* The transcription factor IRF1 and guanylate-binding proteins target activation of the AIM2 inflammasome by *Francisella* infection. *Nat. Immunol.* **16**, 467–475 (2015).
- Boussemer, L. *et al.* eIF4F is a nexus of resistance to anti-BRAF and anti-MEK cancer therapies. *Nature* **513**, 105–109 (2014).
- Karki, R. *et al.* Concerted activation of the AIM2 and NLRP3 inflammasomes orchestrates host protection against *Aspergillus* infection. *Cell Host Microbe* **17**, 357–368 (2015).



Extended Data Figure 1 | See next page for caption.

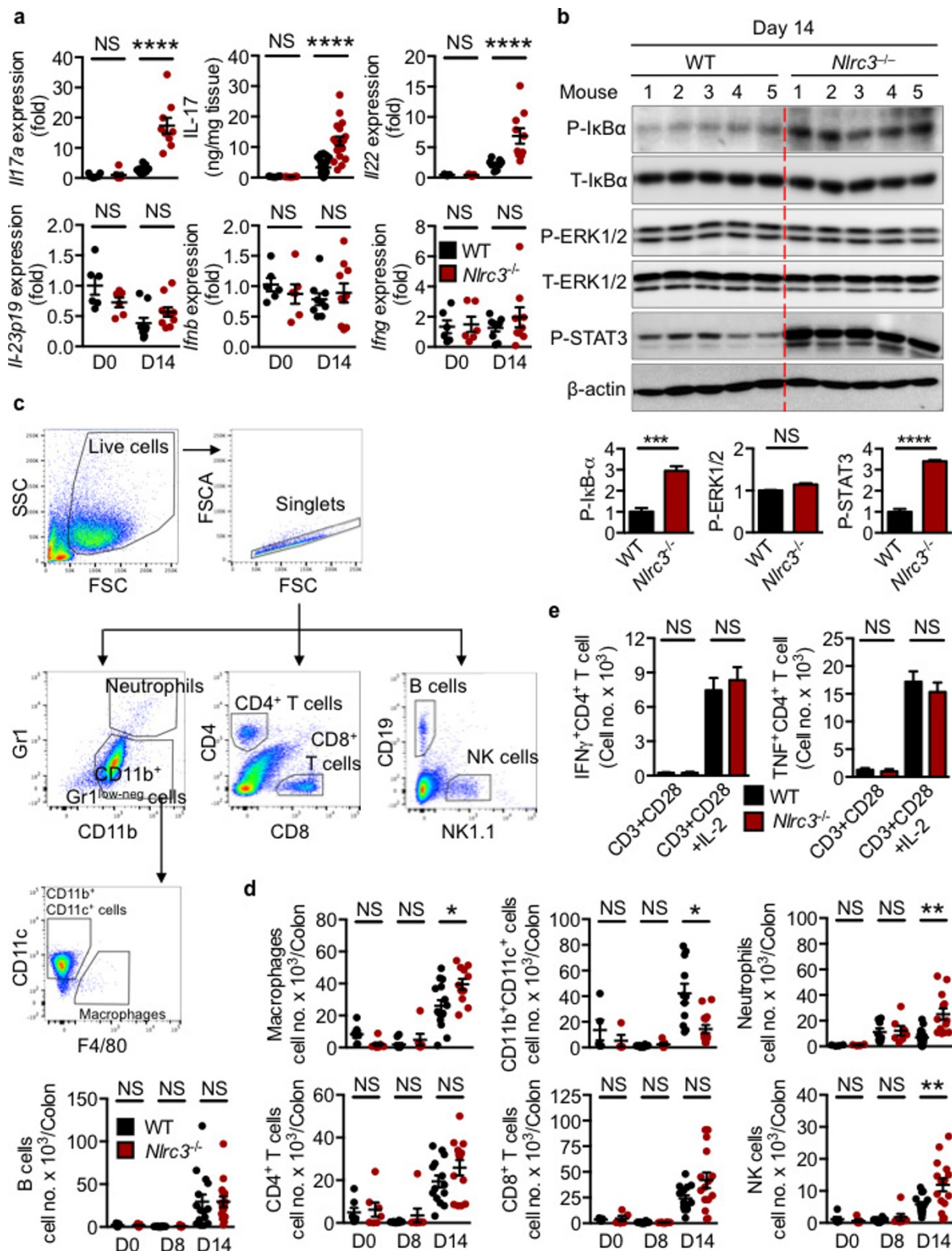
Extended Data Figure 1 | NLRC3 prevents colitis-associated colorectal tumorigenesis. **a**, Timeline for azoxymethane (AOM) and DSS treatment. **b**, Relative expression levels of the gene encoding NLRC3 in tumour and non-tumour tissue in the colon of wild-type mice 80 days after azoxymethane injection. **c**, Targeting strategy used to generate *Nlrc3*^{-/-} mice and PCR analysis for the gene encoding NLRC3 in wild-type C57BL/6 mice, *Nlrc3*^{+/-} mice and *Nlrc3*^{-/-} mice. The primers P1 (which binds a region between exon 1 and exon 2) and P2 (which binds a region between exon 3 and exon 4) were designed for 'PCR1' such that it generates a 4,804-bp PCR fragment for the wild-type allele and a 2,309-bp fragment for the knockout (KO) allele. However, PCR1 cannot differentiate heterozygote (HT) and knockout mice because the knockout

2,309-bp fragment outcompetes the wild-type 4,804-bp fragment. Therefore, we designed primers P3 and P4 for use in PCR2 to amplify a 940-bp fragment from exon 3 to confirm its presence in wild-type and HET mice and its absence in knockout mice. **d**, Histological scores of the colon tissue in wild-type and *Nlrc3*^{-/-} mice 80 days after azoxymethane injection. **e**, Percentages of mice with dysplasia 80 days after injection of azoxymethane. **f**, Percentages of mice with adenocarcinoma 80 days after injection of azoxymethane. **g**, Haematoxylin and eosin staining of colon crypts. Scale bar, 100 µm. Each symbol represents an individual mouse (**b**, **d**). **** $P < 0.0001$; NS, not statistically significant by one-way ANOVA (**b**) or two tailed *t*-test (**d**). Data represent two independent experiments (**b**, **d-g**) and are presented as mean ± s.e.m. (**b**, **d**).



Extended Data Figure 2 | NLRC3 dampens intestinal inflammation.
a, Body-weight change of mice pooled from three independent experiments. **b**, Images of colon and colon length in wild-type mice and *Nlr3*^{-/-} mice at day 14. **c**, Histological scores at day 14. **d**, Levels of IL-18 and IL-1 β in colon tissue at days 14 and 80. **e**, **f**, Levels of IL-6, TNF, G-CSF, KC, MCP-1 and MIP-1 α in colon tissue at days 14 and 80. **g**, Relative expression of genes encoding IL-6, TNF, G-CSF and KC in colon

tissue of untreated wild-type and *Nlr3*^{-/-} mice and in wild-type and *Nlr3*^{-/-} mice at day 14. **h**, Levels of IL-6, G-CSF, KC and MIP-1 α in sera of untreated wild-type and *Nlr3*^{-/-} mice and in wild-type and *Nlr3*^{-/-} mice at days 14 and 80. Each symbol represents an individual mouse (**b–h**). ** $P < 0.01$; **** $P < 0.0001$; NS, not statistically significant by one-way ANOVA (**a**) or two tailed *t*-test (**b–h**). Data represent three independent experiments (**a–h**) and are presented as mean \pm s.e.m. in **a–h**.

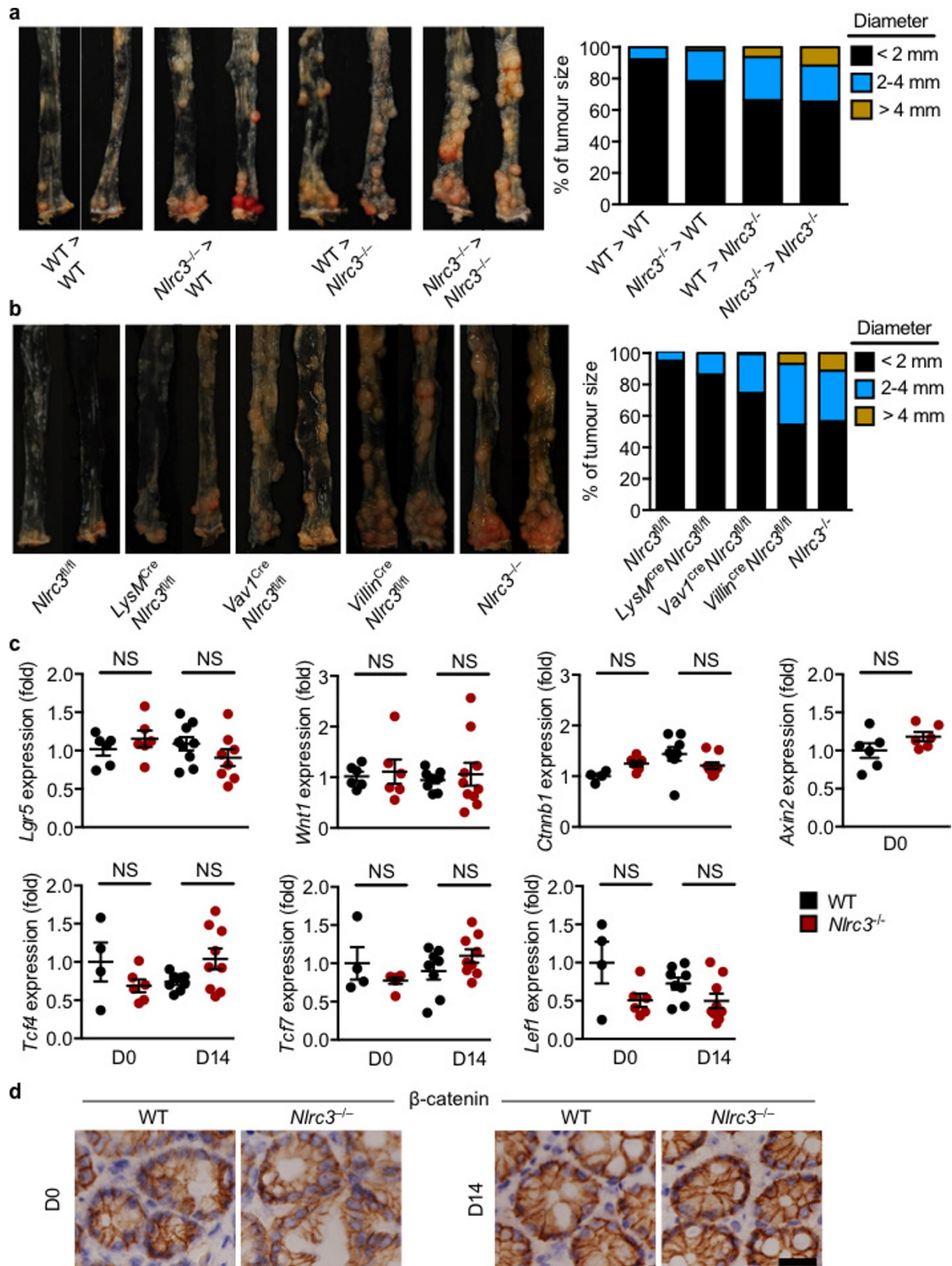


Extended Data Figure 3 | NLRC3 governs colorectal tumorigenic susceptibility via inflammatory mediators and immune cells.

a, Relative expression of genes encoding IL-17a, levels of the IL-17 protein, and relative expression of genes encoding IL-22, IL-23p19, IFN β and IFN γ in colon tissue of untreated wild-type and *Nlrc3*^{-/-} mice and in wild-type and *Nlrc3*^{-/-} mice at day 14. **b**, Immunoblot analysis of phosphorylated and total I κ B α (P-I κ B α and T-I κ B α), ERK1 and ERK2 (P-ERK1/2 and T-ERK1/2), phosphorylated STAT3 (P-STAT3), and β -actin (loading control) in colon tissue of wild-type and *Nlrc3*^{-/-} mice 14 days after injection of azoxymethane (top). The protein band intensity was normalized to the total protein counterpart and/or β -actin, and

expressed relative to that of wild-type controls, set at 1 (bottom).

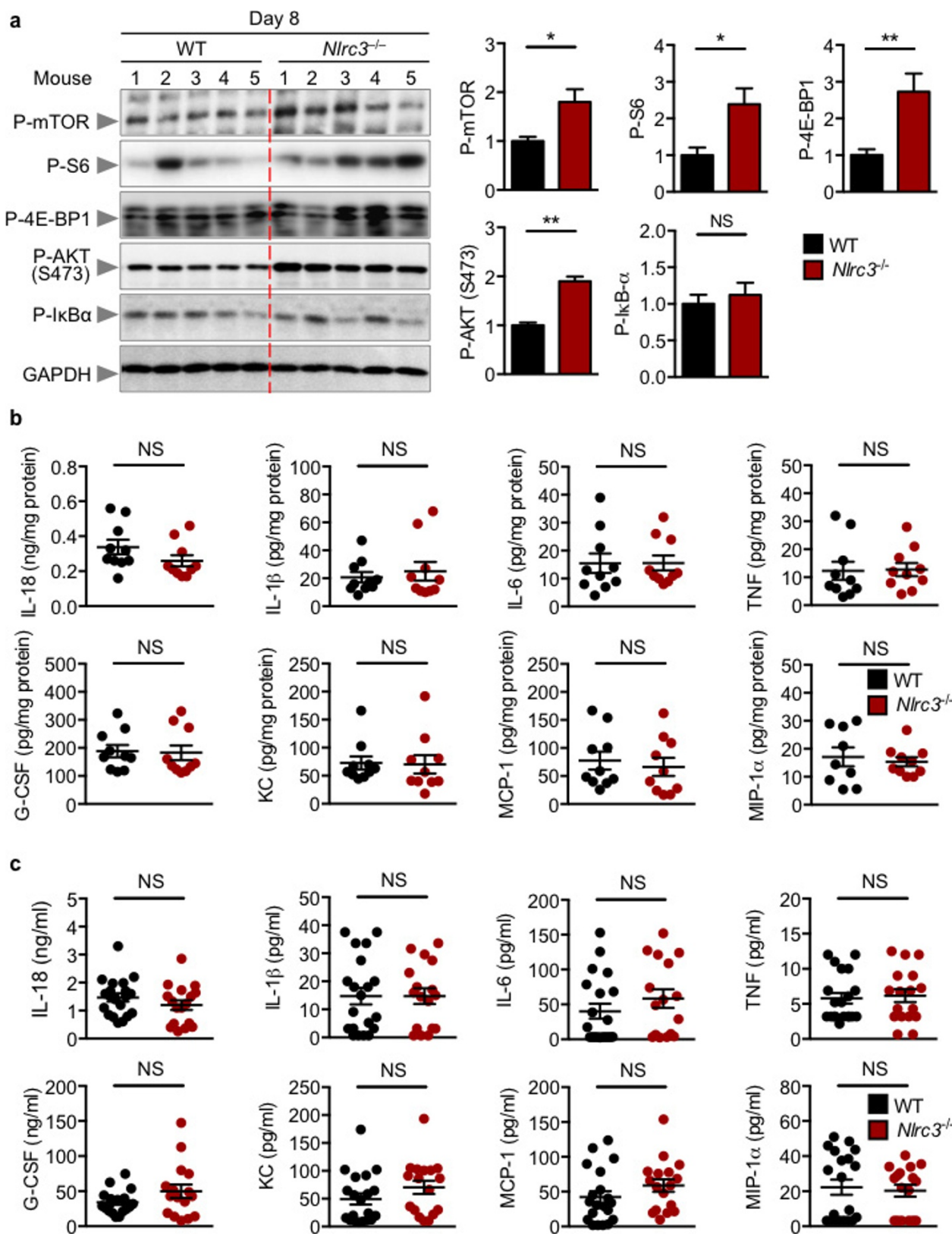
c, Gating strategies used to generate data in **d**. **d**, Number of macrophages, CD11b⁺CD11c⁺ cells, neutrophils, B cells, CD4⁺ T cells, CD8⁺ T cells and natural killer cells per colon in wild-type and *Nlrc3*^{-/-} mice at days 8 and 14. **e**, Splenocytes from wild-type and *Nlrc3*^{-/-} mice were stimulated with CD3, CD28, and IL-2 and intracellular staining was performed for IFN γ and TNF. * $P < 0.05$; ** $P < 0.01$; *** $P < 0.001$; **** $P < 0.0001$; NS, not statistically significant by two-tailed *t*-test (**a**, **d**, **e**). Data pooled from two independent experiments (**a**) or represent one experiment representative of two independent experiments (**b**–**e**) and are presented as mean \pm s.e.m. in **a**, **d**, **e**.



Extended Data Figure 4 | The inhibitory effect of NLRC3 is more dominant in intestinal epithelial cells than in haematopoietic cells.

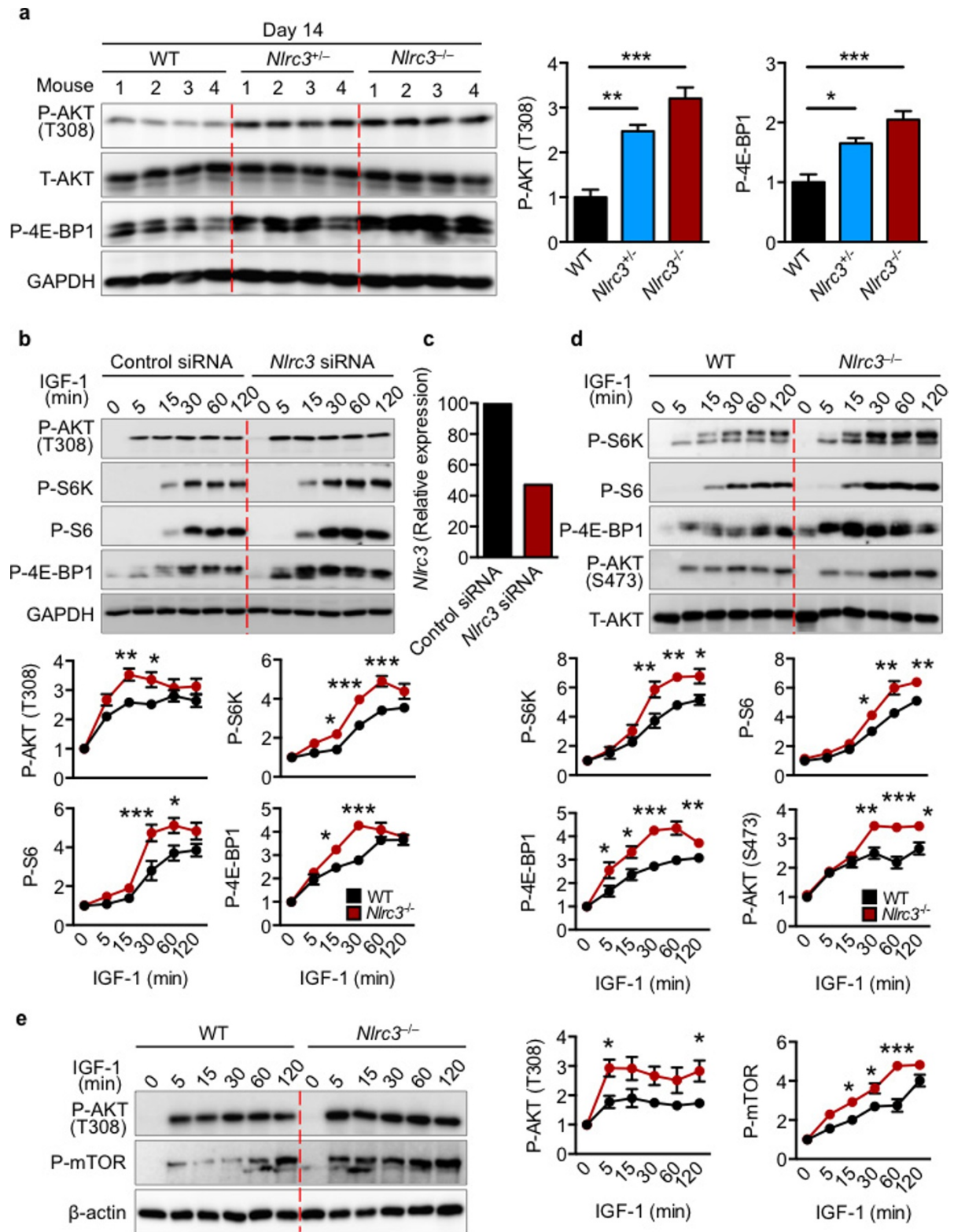
a, Left panel shows colon tumours in, from left to right, wild-type ($n = 10$); $Nlrc3^{-/-} \rightarrow$ wild-type ($n = 9$); wild-type $\rightarrow Nlrc3^{-/-}$ ($n = 8$); $Nlrc3^{-/-} \rightarrow Nlrc3^{-/-}$ ($n = 9$) bone-marrow chimeric mice at day 80. Percentages of the tumour size of mice are shown on the right. **b**, Left panel shows colon tumours in littermate $Nlrc3^{fl/fl}$ ($n = 8$), $LysM^{cre}Nlrc3^{fl/fl}$ ($n = 11$), $Vav1^{cre}Nlrc3^{fl/fl}$ ($n = 9$), $Villin1^{cre}Nlrc3^{fl/fl}$ ($n = 7$) and $Nlrc3^{-/-}$ ($n = 8$) mice at day 80. The percentages of tumours of each size of each

mouse type are shown on the right. **c**, Relative expression of genes encoding LGR5, WNT1, β -catenin ($Ctnnb1$), Axin2, TCF4, TCF7, and LEF1 in colon tissue of untreated wild-type and $Nlrc3^{-/-}$ mice or in wild-type and $Nlrc3^{-/-}$ mice at day 14. **d**, Immunohistochemical staining of β -catenin in colon tissue of wild-type and $Nlrc3^{-/-}$ mice. Scale bar, $20 \mu\text{m}$. Each symbol represents one mouse (**c**). NS, not statistically significant by two-tailed t -test. Data represent two independent experiments and are presented as mean \pm s.e.m. in **c**.



Extended Data Figure 5 | Dysregulation of mTOR signalling precedes dysregulation of NF- κ B signalling. **a**, Immunoblot analysis of phosphorylated mTOR, S6, 4E-BP1, AKT and I κ B α , and GAPDH (loading control) in colon tissue of wild-type and *Nlr3*^{-/-} mice at day 8 (left). The protein band intensity was normalized to GAPDH and expressed as a level relative to that of the wild-type controls, set at 1 (right). **b**, Levels of IL-18,

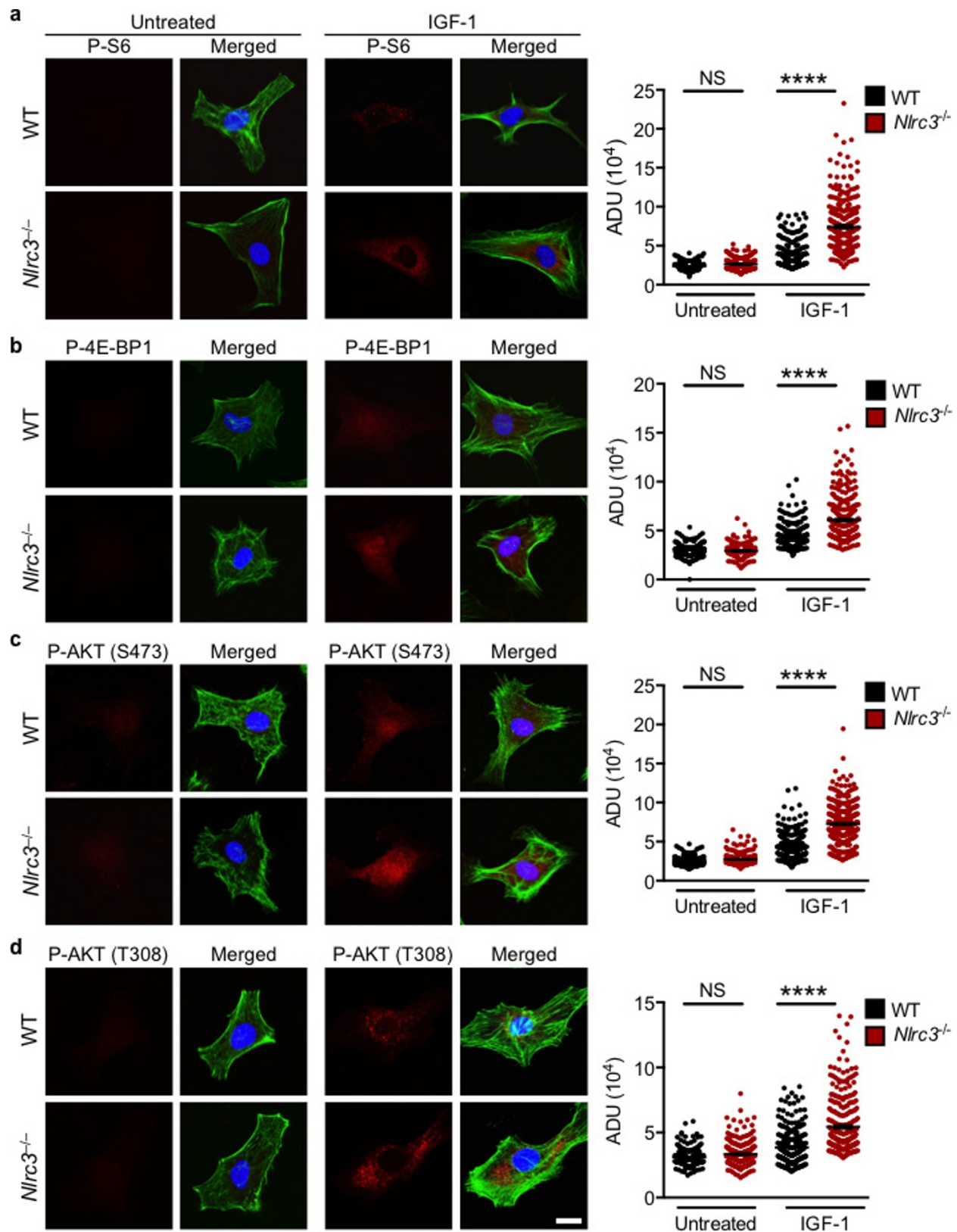
IL-1 β , IL-6, TNF, G-CSF, KC, MCP-1 and MIP-1 α in colon tissue at day 8. **c**, Levels of IL-18, IL-1 β , IL-6, TNF, G-CSF, KC, MCP-1 and MIP-1 α in sera. Each symbol represents an individual mouse (**b**, **c**). * $P < 0.05$; ** $P < 0.01$; NS, not statistically significant by two-tailed *t*-test (**a**–**c**). Data represent two independent experiments and are presented as mean \pm s.e.m. in **a**–**c**. For gel source data, see Supplementary Fig. 1.



Extended Data Figure 6 | NLRC3 regulates mTOR activity.

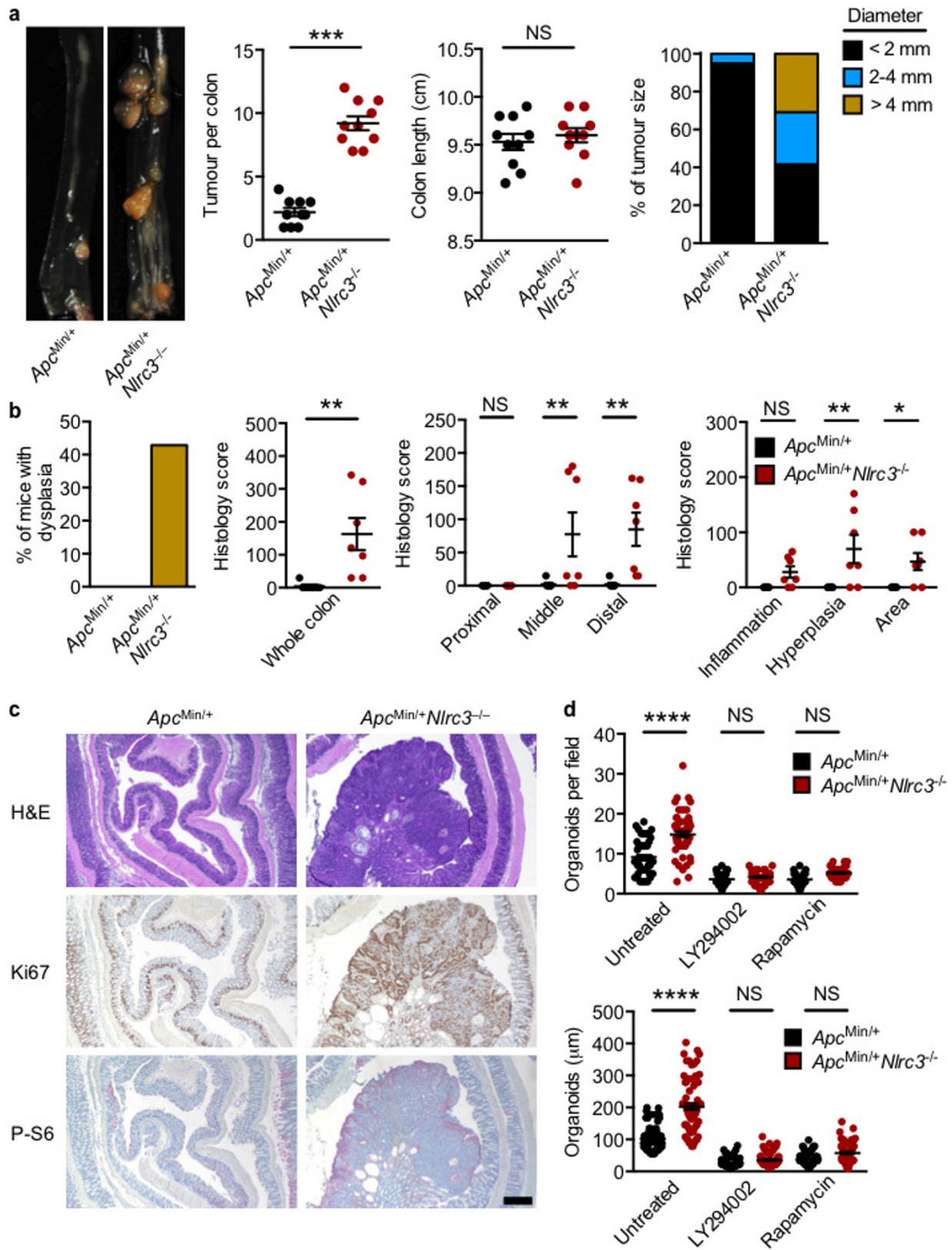
a, Immunoblot analysis of phosphorylated AKT, total AKT, phosphorylated 4E-BP1 and GAPDH (loading control) in the colon tissue of wild-type, *Nlrc3*^{+/-} and *Nlrc3*^{-/-} mice at day 14. The protein-band intensity was normalized to the total protein counterpart and/or the loading control and expressed relative to that of wild-type controls, set at 1 (right). **b**, Immunoblot analysis of phosphorylated AKT, S6K, S6 and 4E-BP1, and GAPDH (loading control) in wild-type fibroblasts transfected with a control siRNA or *Nlrc3* siRNA left untreated or treated with IGF-1 (top). Densitometry analysis as in **a** over 120 min (bottom). **c**, Relative expression of the gene encoding NLRC3 in wild-type fibroblasts

transfected with a control siRNA or compared with wild-type fibroblasts transfected with an *Nlrc3* siRNA. **d**, Immunoblotting of phosphorylated S6K, S6, 4E-BP1, AKT, and total AKT in primary fibroblasts either left untreated or treated with IGF-1 (top). Densitometry analysis as in **a** (bottom). **e**, Immunoblotting of phosphorylated AKT and mTOR, and β -actin (loading control) in primary fibroblasts either left untreated or treated with IGF-1 (left). Densitometry analysis as in **b** (right). * $P < 0.05$; ** $P < 0.01$; *** $P < 0.001$ by one-way ANOVA (**a**, **b**, **d**, **e**). Data are from one experiment representative of two (**a**, **c**) or four independent experiments (**b**, **d** and **e**) and are presented as mean \pm s.e.m. in **a**, **b**, **d**, **e**. For gel source data, see Supplementary Fig. 1.



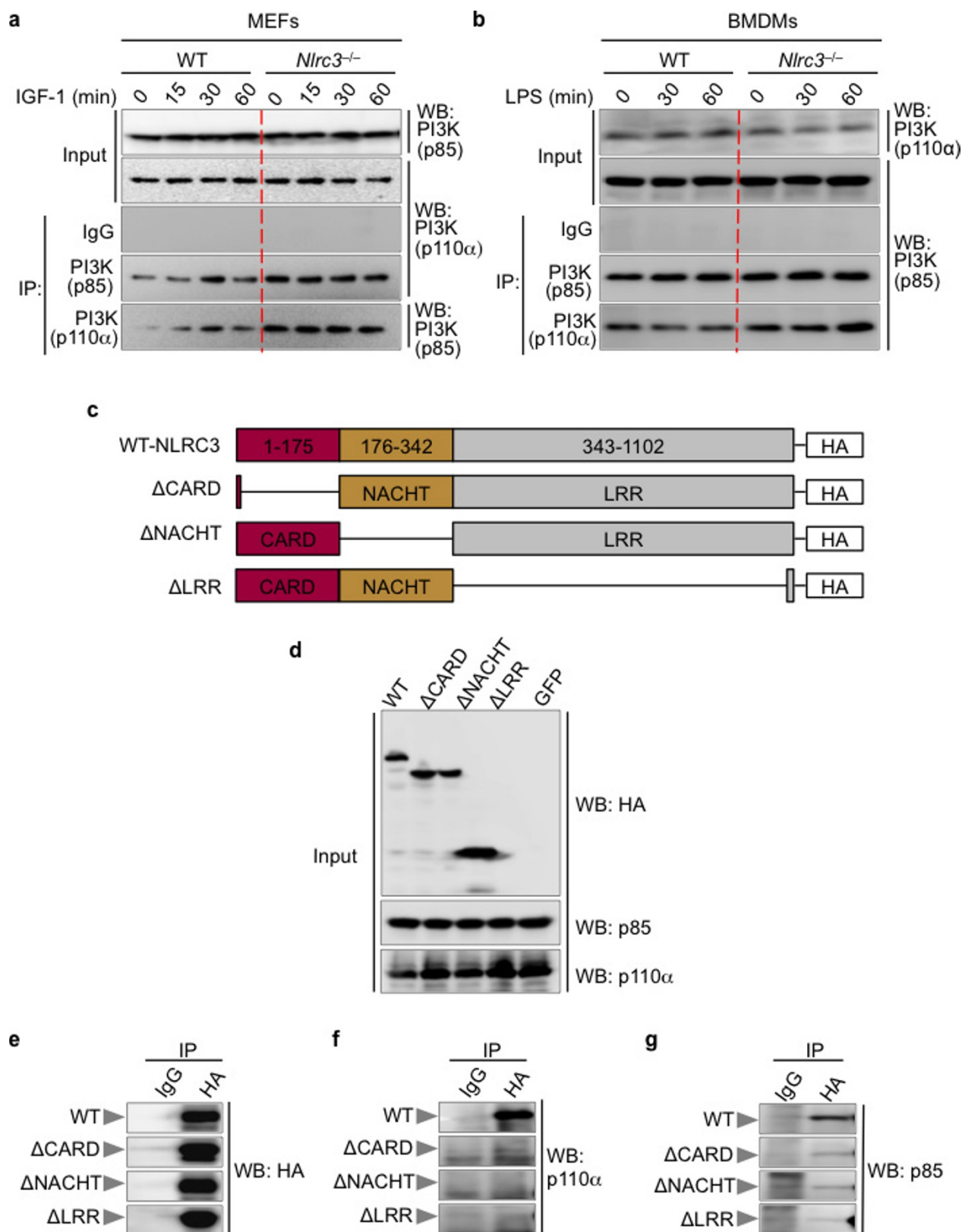
Extended Data Figure 7 | NLRC3 regulates mTOR activity in fibroblasts. a–d, Immunofluorescent stain of phosphorylated S6 (a), 4E-BP1 (b), AKT (c), and AKT (d) in primary fibroblasts either left untreated or treated with IGF-1 for 30 min is shown in the left panels. Quantification of the fluorescence intensity in each cell ($n = 150$ or more)

is shown in the right panels. ADU, average density unit. Scale bar, $20\mu\text{m}$. Each symbol represents an individual cell. **** $P < 0.0001$; NS, not statistically significant by two-tailed t -test. Data represent one experiment representative of two independent experiments and are presented as mean \pm s.e.m.



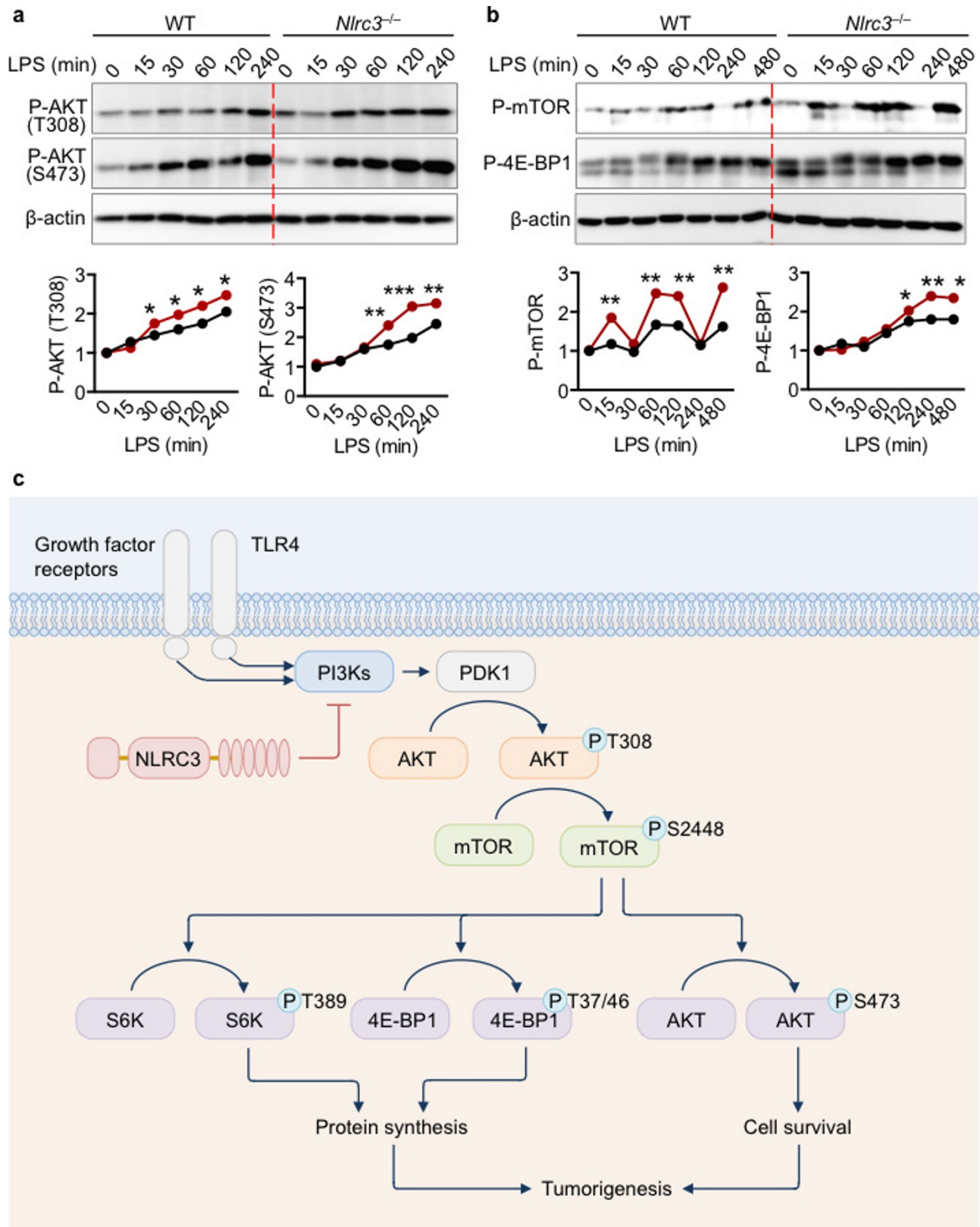
Extended Data Figure 8 | NLRC3 prevents colorectal cancer in an *Apc^{Min/+}* model of tumorigenesis. **a**, Images of colon tumours (left), tumour number and colon length (middle), and size (right) of 120-day-old littermate *Apc^{Min/+}* and *Apc^{Min/+} Nlrc3^{-/-}* mice. **b**, Percentage of mice with dysplasia (left), total histology scores (middle), and histology scores of different parts of colon and different parameters (right) of mice in **a**. **c**, Haematoxylin and eosin (H&E, top), Ki67 (middle) and phosphorylated S6

(P-S6, bottom) staining of colon tumours. Scale bar, 200 µm. **d**, Quantification of the number (top) and size (bottom) of organoids derived from colonic stem cells of *Apc^{Min/+}* and *Apc^{Min/+} Nlrc3^{-/-}* mice left untreated or treated with LY294002 or rapamycin. * $P < 0.05$; ** $P < 0.01$; *** $P < 0.001$; **** $P < 0.0001$; NS, not statistically significant by two-tailed t -test (a, b, d). Data represent two independent experiments and are presented as mean \pm s.e.m. in a, b, d.



Extended Data Figure 9 | NLRC3 disrupts the assembly of the PI3K heterodimeric complex. **a, b**, Immunoprecipitation and comparative analysis of the PI3K signalling complex levels between wild-type and $Nlrc3^{-/-}$ primary mouse embryonic fibroblasts (MEFs; **a**) and BMDMs (**b**). **c**, Schematic representation of the generation of deletion

mutants of NLRC3. **d**, Loading inputs for **e–g**. **e**, Immunoprecipitation of wild-type-NLRC3 and its deletion mutants. **e, f**, Immunoblotting analysis of the interaction between NLRC3 and its mutants with the PI3K-p110 (**f**) and PI3K-p85 (**g**) subunit. Data represent two independent experiments. For gel source data, see Supplementary Fig. 1.



Extended Data Figure 10 | NLRC3 negatively regulates TLR4-induced activation of the PI3K-AKT-mTOR pathway. **a**, Immunoblot analysis of phosphorylated AKT (at Thr308 and Ser473), total AKT and β -actin (loading control) in wild-type and *Nlrc3*^{-/-} bone-marrow-derived macrophages (BMDMs) left untreated or treated with LPS (top). The protein-band intensity was normalized to β -actin, and expressed relative to that of wild-type controls, set at 1 (bottom). **b**, Immunoblot analysis of phosphorylated mTOR, phosphorylated 4E-BP1, and β -actin

(loading control) in wild-type and *Nlrc3*^{-/-} bone-marrow-derived macrophages (BMDMs) left untreated or treated with LPS (top). Densitometry analysis as in **a** (bottom). **c**, A model of the role of NLRC3 in the negative regulation of the PI3K-AKT-mTOR pathway. * $P < 0.05$; ** $P < 0.01$; *** $P < 0.001$ by two-tailed *t*-test (**a**, **b**). Data are from one experiment representative of four independent experiments and are presented as mean \pm s.e.m. in **a** and **b**. For gel source data, see Supplementary Fig. 1.